AFOSR-TR- 3

Models of the Neuronal Mechanisms of Target Localization of the Barn Owl

AD-A230 410

John Pearson, Project Director
David Sarnoff Research Center
Princeton, NJ 08543-5300

December 1990

Annual Technical Report - Fiscal Year 1989

Contract No.: F49620-89-C-0131

Air Force
Office of Scientific Research

REPORT DOCUMENTATION PAGE

Form Approved
OMB No. 0704-0188

1. AGENCY USE ONLY (Leave blank)	2. REPORT DATE	3. REPORT TYPE AND DATES COVERED
	December 1990	Annual Tech. Rpt - FY89

4. TITLE AND SUBTITLE
Models of the Neuronal Mechanisms of Target Localization of the Barn Owl

5. FUNDING NUMBERS
C F49620 89-C 0131
PE - 61102F
PR - 2313
TA - A9

6. AUTHOR(S)
John Pearson

7. PERFORMING ORGANIZATION NAME(S) AND ADDRESS(ES)
David Sarnoff Research Center
201 Washington Road
Princeton, NJ 08543-5300

8. PERFORMING ORGANIZATION REPORT NUMBER

9. SPONSORING/MONITORING AGENCY NAME(S) AND ADDRESS(ES)
Dr. Haddad
AFOSR/NL
Bld 410
Bolling AFB, DC 20332

10. SPONSORING/MONITORING AGENCY REPORT NUMBER

11. SUPPLEMENTARY NOTES

12a. DISTRIBUTION/AVAILABILITY STATEMENT
Unlimited

12b. DISTRIBUTION CODE

13. ABSTRACT (Maximum 200 words)

The major concern of this year's research was modeling the neural systems of the barn owl that determine the elevation of sound sources. Models of the nucleus ventralis lemnisci lateralis pars posterior (VLVp) and the lateral shell of the central nucleus of the inferior colliculus (ICL) were developed. Computer simulations were performed that demonstrated that these models could account for the most salient experimental phenomena. In addition, many intriguing expermental predictions were made. These results were presented at three scientific conferences, at two departmental colloquia, and at one laboratory seminar. Papers will be published from two of these conferences, and several manuscripts are under preparation for publication in peer-reviewed journals. Collaboration was established with experimental neuroscientists within the Konishi Laboratory at CalTech. Future work with these individuals will test predictions of the models, and hopefully lead to a closed-loop interaction between theory and experiment. Another project just beginning is modeling of the system that determines the azimuth of sound sources. Preliminary results indicate that a tuned resonator may be a good model for nucleus laminaris, which generates a representation of the phase delay between sounds

14. SUBJECT TERMS	15. NUMBER OF PAGES
	7
	16. PRICE CODE

17. SECURITY CLASSIFICATION OF REPORT	18. SECURITY CLASSIFICATION OF THIS PAGE	19. SECURITY CLASSIFICATION OF ABSTRACT	20. LIMITATION OF ABSTRACT
Unclassified	Unclassified	Unclassified	

arriving at the two ears. Work on this project involves collaboration with the Princeton University subcontractor.

Accession For	
NTIS GRA&I	☑
DTIC TAB	☐
Unannounced	☐
Justification	
By	
Distribution/	
Availability Codes	
Dist	Avail and/or Special
A-1	

Keywords: Auditory nerve/reflexes; Birds/brain; Sound/[illegible]; Computerized simulation; Neurobiology; Auditory perception

I. BACKGROUND

The barn owl can hunt in total darkness, recognizing and locating prey by hearing alone. One component of this behavior is a very accurate head-orienting response to salient sounds (the head must rotate as the eyes are immobile). This head saccade centers the sound-producing object for closer visual and acoustic scrutiny, prior to aerial attack. Study of this system promises to reveal general principles of the nervous system's approach to three types of problems: sensory encoding and processing, multi-sensory integration, and sensorimotor interaction. Considerable progress has been made in the last 18 years in determining the acoustic and neural bases of the head saccade.

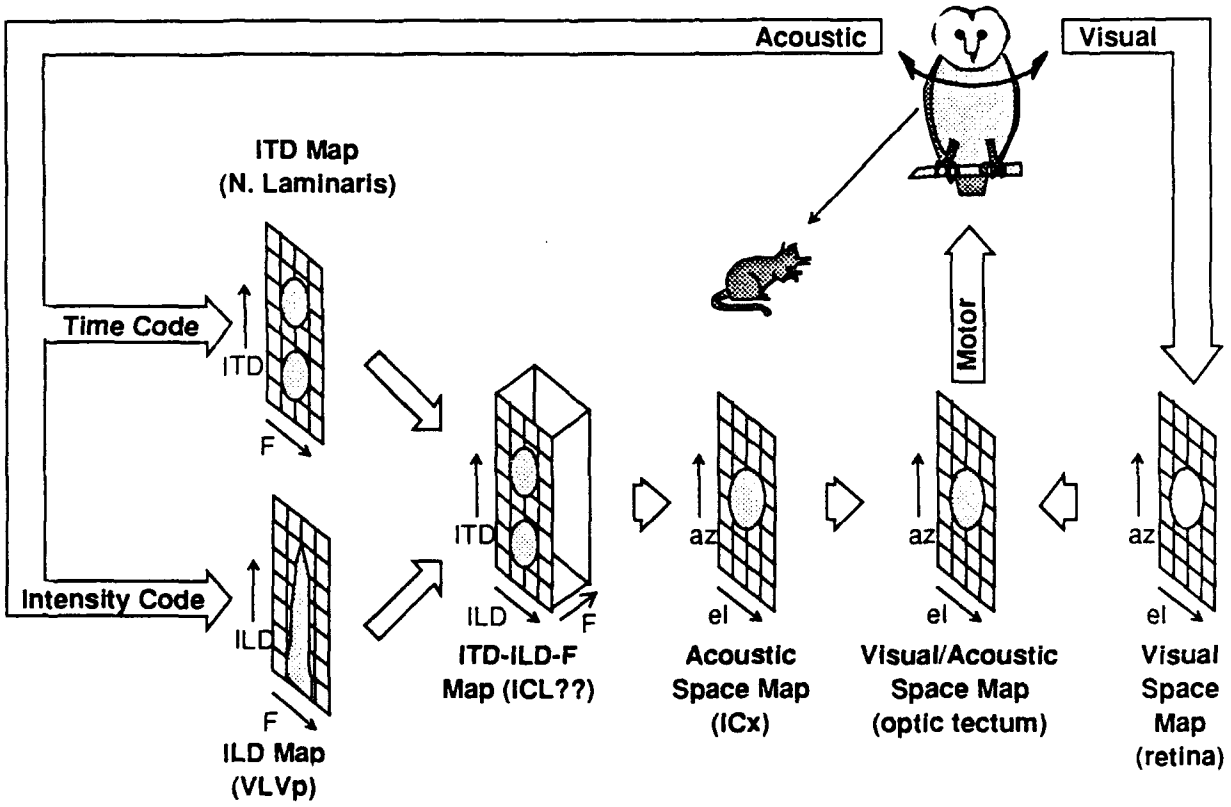

Fig. 1 Overview of the neural system for auditory localization of the barn owl. The grids indicate the map-like representation of information at each processing stage. Acronyms such as VLVp, ICL, and ICx are defined in the text. Arrows indicate the direction of signal flow.

It is known that (see Fig. 1, above): the azimuth and elevation of the sound source direction are encoded at the periphery by, respectively, the inter-aural time difference (ITD) and the inter-aural level difference (ILD); sound intensity and timing information is processed by two parallel

streams before being recombined in a map-like representation of sound direction in the inferior colliculus (ICx); the optic tectum contains a fused visual/auditory/motor representation of stimulus and head saccade direction. The visual/auditory sensory fusion is dynamically recalibrated while the head is growing, with the auditory map in the tectum adapting to realign with the tectal visual map.

II. OBJECTIVES

The purpose of this project is to further the understanding of this system through the development of biophysical and computational models and computer simulations. This work will produce explicit, testable predictions for neuroscience. In addition, it is expected that this research will lead to new artificial neural network designs, with applications for signal processing, sensory fusion, and sensorimotor integration. The following is the Statement of Work (for Year 1) contained in the project proposal:

Task 1 Investigate visual/acoustic sensory fusion in the barn owl by extending existing model of tectal acoustic plasticity to the case of uncorrelated visual/acoustic stimuli.

Task 2 Construct quantitative model of nucleus laminaris (NL) at the signal processing level, taking into account the known statistical character of the magnocellularis inputs, in order to understand the systems extraction of ITD from phase locked input signals.

Task 3 Develop mathematical versions and computer simulations of our preliminary, qualitative models of the ICx, in order to understand how acoustic cues can be combined to yield information of the spatial location of acoustic targets. This includes models of the ILD map in the VLVp and the ITD map in the ICc-core.

III. STATUS

A. Task 1

This task was not performed this year. We chose to devote most of our time to Task 3, in order to respond in a timely fashion to new experimental results in that area. Work on Task 3 was

judged to be of much more significance at this time. Task 1 will be performed as time and interest dictate.

B. Task 2

Neurons in nucleus laminaris receive input from both nuclei magnocellularis. Magnocellularis neurons generate action potentials that are phase-locked to the stimulus (up to 10 kHz.) and nearly independent of intensity. Laminaris neurons are tuned to a particular frequency band and inter-aural phase difference or time delay. This timing system is remarkably precise, with individual neurons being sensitive to time delays as small as 10 μs. Magnocellularis axons course

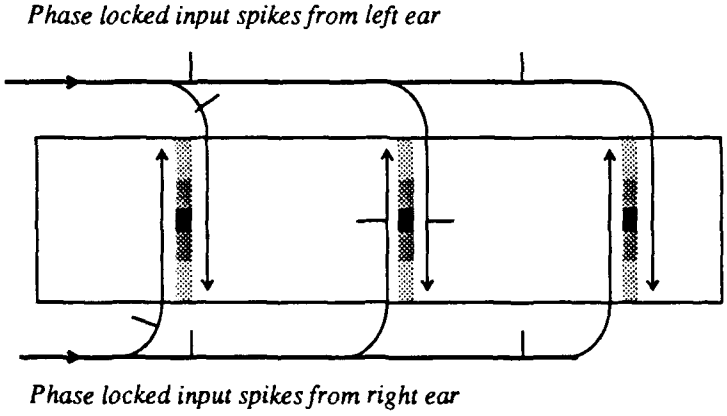

Fig. 2 Schematic diagram of an isofrequency slab of N L. The tick marks on the axons represent action potential pulses in the axons. The shaded bars in NL between the parallel axons represent the degree of excitation of NL neurons, with darker shading representing greater excitation. NL neurons are best stimulated by coincident bilateral input from NM.

through laminaris in a manner suggestive of a coincident delay line mechanism (see Fig. 2, above), and this in fact has been the dominant type of model in the literature. However, these models have been specified at rather high levels of abstraction, in which individual neurons are assumed capable of detecting coincidences in the arrival of action potentials with a resolution of 10 μs. This and a variety of other reasons suggested to us that such models are untenable.

An alternative type of model, investigated in this project, is based on the idea of resonance or temporal priming. That is (in brief simplified form), the effect of an incoming spike is potentiated if it is preceded within a certain time window by another spike, and inhibited otherwise. This

kind of mechanism is known to exist in other neurons, and is suggested for laminaris neurons by the fact that they also phase-lock to the stimulus.

The first test of this general idea was to model an individual laminaris neuron as a damped harmonic oscillator that is kicked by each incoming action potential. Magnocellularis spike trains are modeled by Poisson processes whose rates are modulated by the sound's instantaneous pressure, or as Poisson processes at some constant rate if there is no sound. Presumably, if a real neuron can show some resonance behavior, then some sub-system in the neuron can be modeled this way. The neuron's spike train would somehow be related to the oscillator's phase and amplitude, so that a higher amplitude results in a higher spike rate, and the resulting action potentials occur at some phase of the oscillator's cycle. Simple reasoning shows that this model can qualitatively acount for the data, in particular the monaural response is larger than the out-of-phase binaural response but smaller than the in phase binaural response, and the laminaris neuron's reponse is phase locked. A simulation of the model confirmed these expectations. We anticipate developing this model further in the second fiscal year.

C. Task 3

The intensity processing system was the main focus of study this year. Several anatomical [1] and physiological [2,3] reports on the properties of the nucleus ventralis lemnisci lateralis (VLVp) and the lateral shell of the inferior colliculus (ICL) were published near the start of our program. Our goal was to account for the new physiologically recorded response properties with models that incorporated the new anatomical findings. Of course, the known facts were not sufficient to fully specify the model. Therefore, assumptions were made that were biological and that produced the desired match between the model's simulated response properties and those actually recorded. These assumptions have thus become predictions for experimental verification.

A paper [5] describing the first version of these two models can be found in Appendix A. Subsequent discussions with experimentalists (see Section VI, on page 6) required significant revisions to these models at the level of the detailed anatomy, although the basic computational

model remained the same. A paper [6] describing this second version of the models is in press. and is included in Appendix B. Other recent unpublished experimental findings support the models. In fact, the poster to be presented by Dr. Pearson at the Society of Neuroscience this year [4] concerns the comparison of the models' behavior with the results of recent experiments. However, it is possible that experiments to be performed during the next year may require a revision, not just of the neural wiring diagrams, but of the basic computational models themself.

One indication of the success of a modeling effort is the interest of experimentalists and active collaboration. Such interactions are described in Section VI, page 6.

D. Other Related Work

In addition to his role as consultant to the research effort at Sarnoff, Dr. Sullivan has pursued a number of neurocomputational research topics related to the theme of this contract. Several manuscripts are in preparation (see Section IV, on page 5), and a draft version of one manuscript is included in Appendix C.

IV. PUBLICATIONS

[1] Pearson, J. C., C. D. Spence, and R. Adolphs, "The computation of sound elevation in the barn owl: model and physiology", Society for Neuroscience Abstracts **16** (299.3), 718 (1990).

[2] Pearson, J. C., and C. D. Spence, "Models of the computation of sound source elevation in the barn owl", (in preparation, to be submitted to NETWORK: Computation in Neural Systems).

[3] Pearson, J. C., and C. D. Spence, "Neural maps for subtraction: the computation of sound elevation in the barn owl", (in preparation, to be submitted to Neural Computation).

[4] Pearson, J. C., C. D. Spence and R. Adolphs, "The computation of sound elevation in the barn owl: model and physiology", (in preparation, to be submitted to J. Neurosci).

[5] Spence, C. D., and J. C. Pearson, "The computation of sound source elevation in the barn owl", Advances in Neural Information Processing Systems 2, edited by D. S. Touretzky (Morgan Kaufmann, San Mateo, CA, 1989), pp. 10-17.

[6] Spence, C. D., and J. C. Pearson, "Models of the computation of sound elevation in the barn owl", Proceedings of the Analysis and Modeling of Neural Systems Workshop, Berkely, CA (in press).

[7] Sullivan, W.E., "Temporal hyperacuity and single neuron selectivity: Microsecond time resolution in a neural compartmental model", (in preparation, to be submitted to Biological Cybernetics) .

[8] Sullivan, W.E., "The Square and the Square-Root: Possible neural implementations and their use in sensory and motor information processing", (in preparation, to be submitted to Nature).

[9] Sullivan, W.E., "Spatial and temporal properties of neural subtraction and division: Computational properties of basic cellular operations and network architectures (in preparation, to be submitted to J. Neurosci.).

[10]Sullivan, W.E., "Neural operations and network functions: Possible mechanisms for subtraction and division at membrane, local circuit and molecular levels", (in preparation, to be submitted to J. Neurosci.).

V. PERSONNEL

The principle investigators are J. C. Pearson, Member of the Technical Staff (promoted December 1, 1990 to Group Head) of the David Sarnoff Research Center and Professor W. E. Sullivan of the Biology Department of Princeton University; both institutions are located in Princeton, New Jersey. Dr. Pearson is the project director, and is also involved with research in the applications of artificial neural networks to signal processing problems. Dr. Sullivan, who is an experimental neuroscientist active in this field, serves as a consultant and ensures that the models developed at Sarnoff incorporate the latest findings and are biologically feasible and testable. Dr. Sullivan is also developing neurocomputational models related to the themes of this project. Working with Dr. Pearson at Sarnoff is Dr. C. D. Spence, Member of the Technical Staff.

VI. INTERACTIONS

In October, the first version of the ICL and VLVp models was presented at the Annual Meeting of the Society for Neuroscience, in poster format. R. Adolphs, a graduate student in the Konishi Lab of CalTech, became quite interested in the modeling work, and a working collaboration has ensued. He is a co-author on the poster for this year's Annual Meeting, and on several planned manuscripts.

In November, a slightly improved version of the ICL and VLVp models was presented at the NIPS conference (Neural Information Processing Systems: Natural and Synthetic; held each year in Denver at the end of November), in poster format. A paper was published in the proceedings of the conference [5] (see also appendix A).

In February, Dr. Pearson was invited to give a lecture to the Department of Physiology and Neurobiology of the University of Connecticut at Storrs. The invitation was extended by Dr. Moiseff, who is an active barn owl experimentalist that has taken an interest in the modeling efforts of this project. There is an ongoing exchange of information and idea's between Dr. Moiseff and the personnel of this program. In fact, it was some unpublished observations of Dr. Moiseff that motivated the modeling approach to N. laminaris discussed above.

In May, R. Adolphs invited Drs. Pearson and Spence to the Konishi lab to give a talk, and to continue discussions about future collaborative work. Here certain unpublished observations were learned that required significant revisions in the wiring diagrams of the VLVp and ICL models.

In August, Drs. Pearson and Spence presented a poster (paper in press, see appendix B) about the revised VLVp and ICL models at the first "Analysis and Modelling of Neural Systems" workshop, held in Berkely, CA. They also gave a talk on the VLVp and ICL models to the Knudsen lab at Stanford.

VII. REFERENCES

[1] Carr, C. E., I. Fujita, and M. Konishi, "Distribution of GABAergic neurons and terminals in the auditory system of the barn owl", The Journal of Comparative Neurology **286**, 190-207 (1989).

[2] Fujita, I., and M. Konishi, "Transition from single to multiple frequency channels in the processing of binaural disparity cues in the owl's midbrain", Society for Neuroscience Abstracts **15**: 114 (1989).

[3] Manley, G. A., C. Koppl, and M. Konishi, "A neural map of interaural intensity differences in the brain stem of the barn owl", The Journal of Neuroscience **8**(8), 2665-2676 (1988).

[4] Pearson, J. C., C. D. Spence, and R. Adolphs, "The computation of sound elevation in the barn owl: model and physiology", Society for Neuroscience Abstracts **16** (299.3), 718 (1990).

[5] Spence, C. D., and J. C. Pearson, "The computation of sound source elevation in the barn owl", Advances in Neural Information Processing Systems 2, edited by D. S. Touretzky (Morgan Kaufmann, San Mateo, CA, 1989), pp. 10-17.

[6] Spence, C. D., and J. C. Pearson, "Models of the computation of sound elevation in the barn owl", Proceedings of the Analysis and Modeling of Neural Systems Workshop, Berkely, CA (in press).

APPENDIX A

The Computation of Sound Source Elevation in the Barn Owl

Advances in Neural Information Processing Systems II,
ed. David S. Touretzky,
Morgan Kauffmann, 1990

The Computation of Sound Source Elevation in the Barn Owl

Clay D. Spence
John C. Pearson
David Sarnoff Research Center
CN5300
Princeton, NJ 08543-5300

ABSTRACT

The midbrain of the barn owl contains a map-like representation of sound source direction which is used to precisely orient the head toward targets of interest. Elevation is computed from the interaural difference in sound level. We present models and computer simulations of two stages of level difference processing which qualitatively agree with known anatomy and physiology, and make several striking predictions.

1 INTRODUCTION

The auditory system of the barn owl constructs a map of sound direction in the external nucleus of the inferior colliculus (ICx) after several stages of processing the output of the cochlea. This representation of space enables the owl to orient its head to sounds with an accuracy greater than any other tested land animal [Knudsen, et al, 1979]. Elevation and azimuth are processed in separate streams before being merged in the ICx [Konishi, 1986]. Much of this processing is done with neuronal maps, regions of tissue in which the position of active neurons varies continuously with some parameters, e.g., the retina is a map of spatial direction. In this paper we present models and simulations of two of the stages of elevation processing that make several testable predictions. The relatively elaborate structure of this system emphasizes one difference between the sum-and-sigmoid model neuron and real neurons, namely the difficulty of doing subtraction with real neurons. We first briefly review the available data on the elevation system.

To appear in *Advances in Neural Information Processing Systems 2*, the proceedings of the 1989 IEEE Conference on Neural Information Processing Systems — Natural and Synthetic.

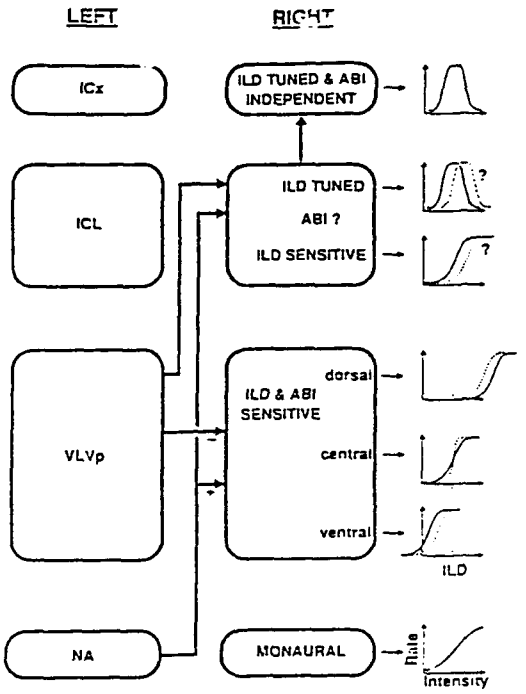

Figure 1: Overview of the Barn Owl's Elevation System. ABI: average binaural intensity. ILD: Interaural level difference. Graphs show cell responses as a function of ILD (or monaural intensity for NA).

2 KNOWN PROPERTIES OF THE ELEVATION SYSTEM

The owl computes the elevation to a sound source from the inter-aural sound pressure level difference (ILD).[1] Elevation is related to ILD because the owl's ears are asymmetric, so that the right ear is most sensitive to sounds from above, and the left ear is most sensitive to sounds from below [Moiseff, 1989].

After the cochlea, the first nucleus in the ILD system is nucleus angularis (NA) (Fig. 1). NA neurons are monaural, responding only to ipsilateral stimuli.[2] Their outputs are a simple spike rate code for the sound pressure level on that side of the head, with firing rates that increase monotonically with sound pressure level over a rather broad range, typically 30 dB [Sullivan and Konishi, 1984].

[1] Azimuth is computed from the interaural time or phase delay.

[2] Neurons in all of the nuclei we will discuss except ICx have fairly narrow frequency tuning curves.

Each NA projects to the contralateral nucleus ventralis lemnisci lateralis pars posterior (VLVp). VLVp neurons are excited by contralateral stimuli, but inhibited by ipsilateral stimuli. The source of the ipsilateral inhibition is the contralateral VLVp [Takahashi, 1988]. VLVp neurons are said to be sensitive to ILD, that is their ILD response curves are sigmoidal, in contrast to ICx neurons which are said to be tuned to ILD, that is their ILD response curves are bell-shaped. Frequency is mapped along the anterior-posterior direction, with slabs of similarly tuned cells perpendicular to this axis. Within such a slab, cell responses to ILD vary systematically along the dorsal-ventral axis, and show no variation along the medio-lateral axis. The strength of ipsilateral inhibition[3] varies roughly sigmoidally along the dorsal-ventral axis, being nearly 100% dorsally and nearly 0% ventrally. The ILD threshold, or ILD at which the cell's response is half its maximum value, varies from about 20 dB dorsally to -20 dB ventrally. The response of these neurons is not independent of the average binaural intensity (ABI), so they cannot code elevation unambiguously. As the ABI is increased, the ILD response curves of dorsal cells shift to higher ILD, those of ventral cells shift to lower ILD, and those of central cells keep the same thresholds, but their slopes increase (Fig. 1) [Manley, et al, 1988].

Each VLVp projects contralaterally to the lateral shell of the central nucleus of the inferior colliculus (ICL) [T. T. Takahashi and M. Konishi, unpublished]. The ICL appears to be the nucleus in which azimuth and elevation information is merged before forming the space map in the ICx [Spence, et al, 1989]. At least two kinds of ICL neurons have been observed, some with ILD-sensitive responses as in the VLVp and some with ILD-tuned responses as in the ICx [Fujita and Konishi, 1989]. Manley, Köppl and Konishi have suggested that inputs from both VLVps could interact to form the tuned responses [Manley, et al, 1988]. The second model we will present suggests a simple method for forming tuned responses in the ICL with input from only one VLVp.

3 A MODEL OF THE VLVp

We have developed simulations of matched iso-frequency slabs from each VLVp in order to investigate the consequences of different patterns of connections between them. We attempted to account for the observed gradient of inhibition by using a gradient in the number of inhibitory cells. A dorsal-ventral gradient in the number density of different cell types has been observed in staining experiments [C. E. Carr, et al, 1989], with GABAergic cells[4] more numerous at the dorsal end and a non-GABAergic type more numerous at the ventral end.

To model this, our simulation has a "unit" representing a group of neurons at each of forty positions along the VLVp. Each unit has a voltage v which obeys the equation

$$C\frac{dv}{dt} = -g_L(v - v_L) - g_E(v - v_E) - g_I(v - v_I).$$

[3] measured functionally, not actual synaptic strength. See [Manley, et al, 1988] for details.

[4] GABAergic cells are usually thought to be inhibitory.

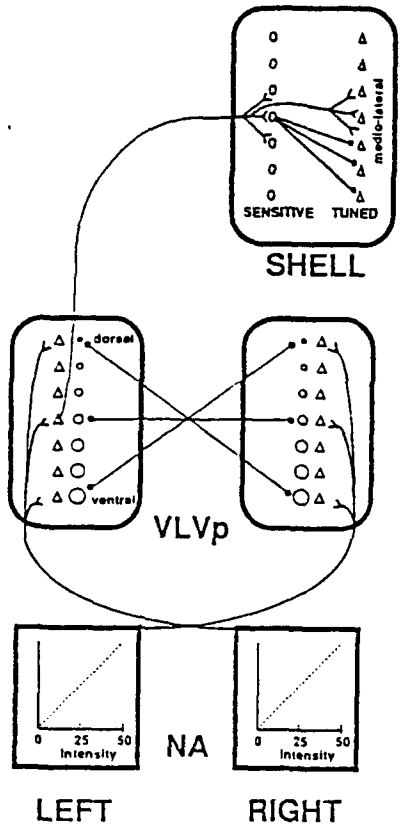

Figure 2: Models of Level Difference Computation in the VLVps and Generation of Tuned Responses in the ICL. Sizes of Circles represent the number density of inhibitory neurons, while triangles represent excitatory neurons.

This describes the charging and discharging of the capacitance C through the various conductances g, driven by the voltages v_N, all of these being properties of the cell membrane. The subscript L refers to passive leakage variables, E refers to excitatory variables, and I refers to inhibitory variables. These model units have firing rates which are sigmoidal functions of v. The output on a given time step is a number of spikes, which is chosen randomly with a Poisson distribution whose mean is the unit's current firing rate times the length of the time step. g_E and g_I obey the equation

$$\frac{d^2g}{dt^2} = -\gamma\frac{dg}{dt} - \omega^2 g,$$

the equation for a damped harmonic oscillator. The effect of one unit's spike on another unit is to "kick" its conductance g, that is it simply increments the conductance's time derivative by some amount depending on the strength of the connection.

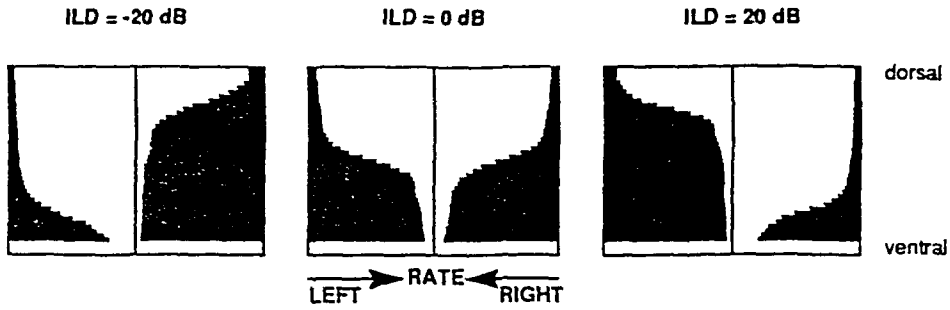

Figure 3: Output of Simulation of VLVps at Several ILDs. Position is represented on the vertical axis. Firing rate is represented by the horizontal length of the black bars.

Inhibitory neurons increment dg_I/dt, while excitatory neurons increment dg_E/dt. γ and ω are chosen so that the oscillator is at least critically damped, and g remains non-negative. This model gives a fairly realistic post-synaptic potential, and the effects of multiple spikes naturally add. The gradient of cell types is modeled by having a different maximum firing rate at each level in the VLVp.

The VLVp model is shown in figure 2. Here, central neurons of each VLVp project to central neurons of the other VLVp, while more dorsal neurons project to more ventral neurons, and conversely. This forms a sort of "criss-cross" pattern of projections. In our simulation these projections are somewhat broad, each unit projecting with equal strength to all units in a small patch. In order for the dorsal neurons to be more strongly inhibited, there must be more inhibitory neurons at the ventral end of each VLVp, so in our simulation the maximum firing rate is higher there and decreases linearly toward the dorsal end. A presumed second neuron type is used for ouput, but we assumed its inputs and dynamics were the same as the inhibitory neurons and so we didn't model them. The input to the VLVps from the two NAs was modeled as a constant input proportional to the sound pressure level ir the corresponding ear. We did not use Poisson distributed firing in this case because the spike trains of NA neurons are very regular [Sullivan and Konishi, 1984]. NA input was the same to each unit in the VLVp.

Figure 3 shows spatial activity patterns of the two simulated VLVps for three different ILDs, all at the same ABI. The criss-cross inhibitory connections effectively cause these bars of activity to compete with each other so that their lengths are always approximately complementary. Figure 4 presents results of both models discussed in this paper for various ABIs and ILDs. The output of VLVp units qualitatively matches the experimentally determined responses, in particular the ILD response curves show similar shifts with ABI. for the different dorsal-ventral positions in the VLVp (see Fig. 3 in [Manley, et al, 1988]). Since the observed non-GABAergic neurons are more numerous at the ventral end of the VLVp and

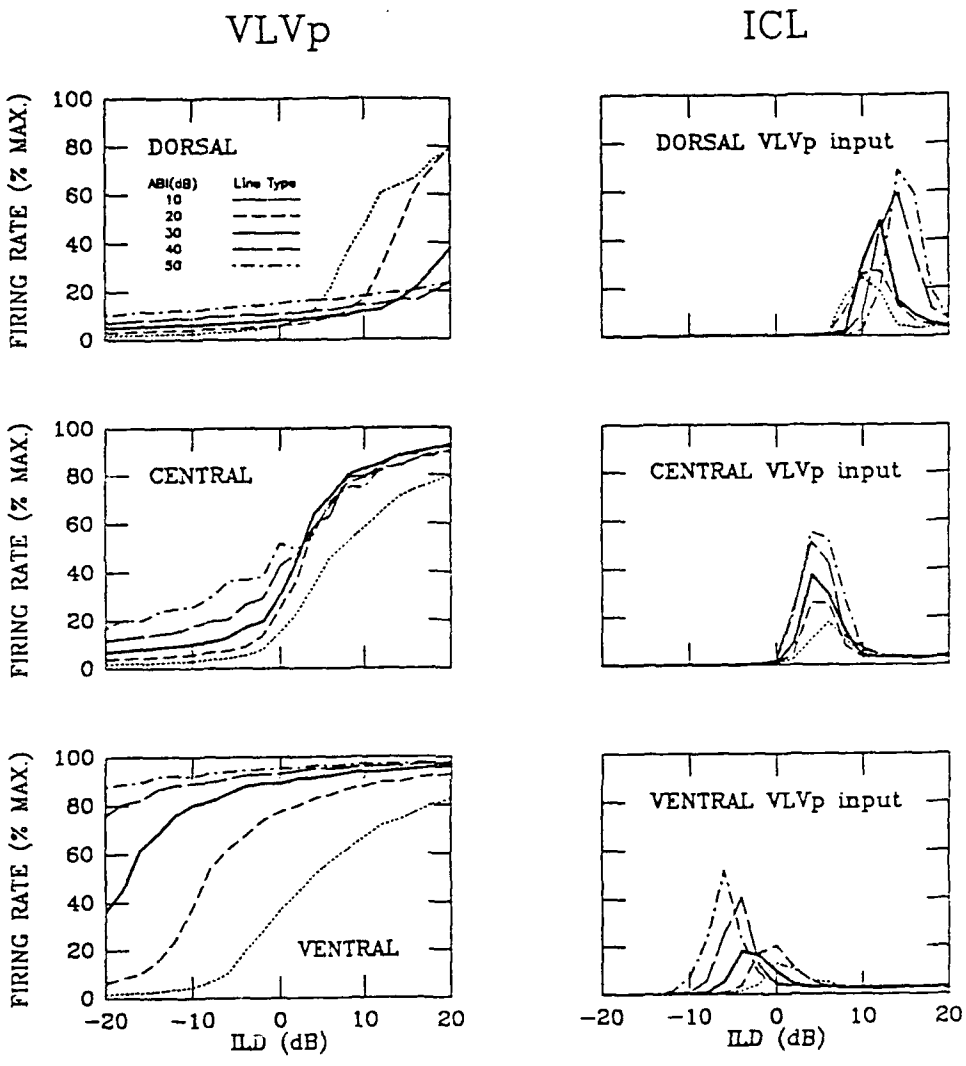

Figure 4: ILD Response Curves of the VLVp and ICL models. Curves show percent of maximum firing rate versus ILD for several ABIs.

our model's inhibitory neurons are also more numerous there, this model predicts that at least some of the non-GABAergic cells in the VLVp are the neurons which provide the mutual inhibition between the VLVps.

4 A MODEL OF ILD-TUNED NEURONS IN THE ICL

In this section we present a model to explain how ICL neurons can be tuned to ILD if they only receive input from the ILD-sensitive neurons in one VLVp. The model essentially takes the derivative of the spatial activity pattern in the VLVp, converting the sigmoidal activity pattern into a pattern with a localized region of activity corresponding to the end of the bar.

The model is shown in figure 2. The VLVp projects topographically to ICL neurons, exciting two different types. This would excite bars of activity in the ICL, except one type of ICL neuron inhibits the other type. Each inhibitory neuron projects to tuned neurons which represent a smaller ILD, to one side in the map. The inhibitory neurons acquire the bar shaped activity pattern from the VLVp, and are ILD-sensitive as a result. Of the neurons of the second type, only those which receive input from the end of the bar are not also inhibited and prevented from firing.

Our simulation used the model neurons described above, with input to the ICL taken from our model of the VLVp. Each unit in the VLVp projected to a patch of units in the ICL with connection strengths proportional to a gaussian function of distance from the center of the patch. (Equal strengths for the connections from a given neuron worked poorly.) The results are shown in figure 4. The model shows sharp tuning, although the maximum firing rates are rather small. The ILD response curves show the same kind of ABI dependence as those of the VLVp model. There is no published data to confirm or refute this, but we know that neurons in the space map in the ICx do not show ABI dependence. There is a direct input from the contralateral NA to the ICL which may be involved in removing ABI dependence, but we have not considered that possibility in this work.

5 CONCLUSION

We have presented two models of parts of the owl's elevation or interaural level difference (ILD) system. One predicts a "criss-cross" geometry for the connections between the owl's two VLVps. In this geometry cells at the dorsal end of either VLVp inhibit cells at the ventral end of the other, and are inhibited by them. Cells closer to the center of one VLVp interact with cells closer to the center of the other, so that the central cells of each VLVp interact with each other (Fig. 2). This model also predicts that the non-GABAergic cells in the VLVp are the cells which project to the other VLVp. The other model explains how the ICL, with input from one VLVp, can contain neurons tuned to ILD. It does this essentially by computing the spatial derivative of the activity pattern in the VLVp. This model predicts that the ILD-sensitive neurons in the ICL inhibit the ILD-tuned neurons in the ICL. Simulations with semi-realistic model neurons show that these models

are plausible, that is they can qualitatively reproduce the published data on the responses of neurons in the VLVp and the ICL to different intensities of sound in the two ears.

Although these are models, they are good examples of the simplicity of information processing in neuronal maps. One interesting feature of this system is the elaborate mechanism used to do subtraction. With the usual model of a neuron, which calculates a sigmoidal function of a weighted sum of its inputs, subtraction would be very easy. This demonstrates the inadequacy of such simple model neurons to provide insight into some real neural functions.

Acknowledgements

This work was supported by AFOSR contract F49620-89-C-0131.

References

C. E. Carr, I. Fujita, and M. Konishi. (1989) Distribution of GABAergic neurons and terminals in the auditory system of the barn owl. *The Journal of Comparative Neurology* 286: 190–207.

I. Fujita and M. Konishi. (1989) Transition from single to multiple frequency channels in the processing of binaural disparity cues in the owl's midbrain. *Society for Neuroscience Abstracts* 15: 114.

E. I. Knudsen, G. G. Blasdel, and M. Konishi. (1979) Sound localization by the barn owl measured with the search coil technique. *Journal of Comparative Physiology* 133:1–11.

M. Konishi. (1986) Centrally synthesized maps of sensory space. *Trends in Neurosciences* April, 163–168.

G. A. Manley, C. Köppl, and M. Konishi. (1988) A neural map of interaural intensity differences in the brain stem of the barn owl. *The Journal of Neuroscience* 8(8): 2665–2676.

A. Moiseff. (1989) Binaural disparity cues available to the barn owl for sound localization. *Journal of Comparative Physiology* 164: 629–636.

C. D. Spence, J. C. Pearson, J. J. Gelfand, R. M. Peterson, and W. E. Sullivan. (1989) Neuronal maps for sensory-motor control in the barn owl. In D. S. Touretzky (ed.), *Advances in Neural Information Processing Systems 1*, 748–760. San Mateo, CA: Morgan Kaufmann.

W. E. Sullivan and M. Konishi. (1984) Segregation of stimulus phase and intensity coding in the cochlear nucleus of the barn owl. *The Journal of Neuroscience* 4(7): 1787–1799.

T. T. Takahashi. (1988) Commissural projections mediate inhibition in a lateral lemniscal nucleus of the barn owl. *Society for Neuroscience Abstracts* 14: 323.

APPENDIX B

Models of the Computation of Elevation in the Barn Owl

To appear in the proceedings of the conference

Analysis and Modelling of Neural Systems,

Berkely, California, July 1990

Models of the Computation of Sound Elevation in the Barn Owl

Clay D. Spence and John C. Pearson
David Sarnoff Research Center
CN5300
Princeton, NJ 08543-5300
cds@as1.sarnoff.com

Abstract

We present a model of the first stage in the part of the barn owl's auditory system which computes the elevation of a sound from the pressure levels at the ears. We also give a detailed description of our simulations of the model. Using several novel techniques, a few seconds of real time on a Sun Sparcstation are sufficeint to simulate 2000 neurons for 100 milliseconds of simulated time. The response properties of the model neurons are a good match to those of real neurons.

Introduction

The barn owl (*tyto alba*) can determine the direction to sources of sound more accurately than any other tested land animal [Knudsen, et al, 1979]. The auditory system of the barn owl constructs a map of sound source direction in the external nucleus of the inferior colliculus (ICx), which is used to orient the head. Elevation and azimuth are processed separately before being merged in the ICx [Konishi, 1986]. The owl computes the elevation to a sound source from the interaural sound pressure level difference (ILD). (Azimuth is computed from the interaural time or phase delay.) Elevation is related to ILD because the owl's ears are asymmetric, so that the right ear is most sensitive to sounds from above, and the left ear is most sensitive to sounds from below [Moiseff, 1989].

The first stage of ILD processing occurs in nucleus ventralis lemnisci lateralis pars posterior (VLVp). VLVp neurons are excited by contralateral stimuli and inhibited by ipsilateral stimuli. The source of excitation is the contralateral cochlear nucleus angularis (NA), whose neurons' outputs are simple spike rate codes for the ipsilateral sound level. Surprisingly, the source of inhibition is not the ipsilateral NA, but the contralateral VLVp [Takahashi, 1988] (Fig. 1). VLVp neurons are said to be sensitive to ILD, meaning their ILD response curves are sigmoidal. Frequency is mapped along the anterior-posterior direction in the VLVp, with slabs of similarly tuned cells perpendicular to this axis. Within such a slab, cell responses to ILD vary systematically along the dorsal-ventral axis, and show no variation along the medio-lateral axis. The strength of ipsilateral inhibition (measured functionally, not actual synaptic strength; see [Manley, et al,

To appear in the proceedings of the conference
Analysis and Modelling of Neural Systems,
Berkeley, California, July 1990.

1988] for details) varies roughly sigmoidally along the dorsal-ventral axis, being nearly 100% dorsally and nearly 0% ventrally. The ILD threshold, or ILD at which the cell's response is half its maximum value, varies from roughly 20 dB dorsally to -20 dB ventrally. The response of these neurons is not independent of the average binaural intensity (ABI), so they cannot code elevation unambiguously. As the ABI is increased, the ILD response curves of dorsal cells shift to higher ILD, those of ventral cells shift to lower ILD, and those of central cells keep the same thresholds, but their slopes decrease [Manley, et al, 1988].

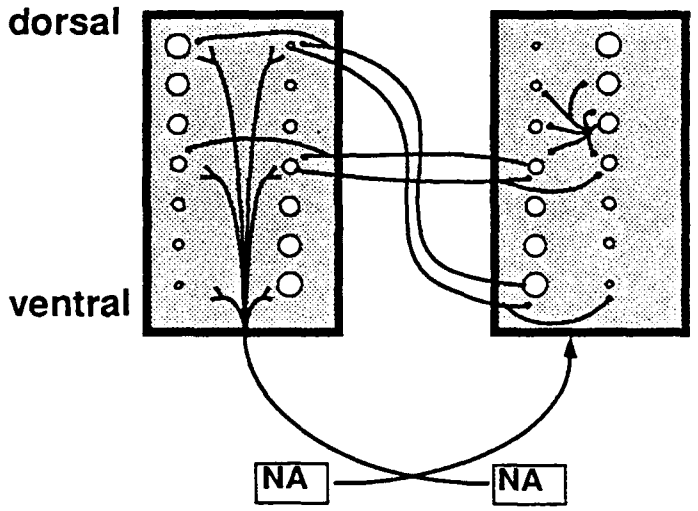

Figure 1. Overview of competitive edge model of VLVp. Circle sizes represent relative numbers of neurons at a given level. Neurons which inhibit the other VLVp and local inhibitory neurons are shown.

The competitive edge model of the VLVp

In an earlier paper [Spence and Pearson, 1990] we predicted a criss-cross pattern of mutual inhibitory connections between the two VLVps, as in figure 1. Independently, T. T. Takahashi has shown that ventral neurons do project to the dorsal end of the VLVp, partially confirming this prediction. The strength of the inhibitory projection varies monotonically along the dorsal-ventral axis, so a given group of neurons which are closer to the ventral end tend to dominate the neurons in the other VLVp to which they are connected, unless those neurons are excited more. For a given ILD and ABI, there is a location in each VLVp, such that they are connected to each other and the difference in the strength with which they inhibit each other is balanced by the difference in excitation, so that the neurons at these locations will have the same firing rate. At other locations one side will dominate, resulting in a bar-shaped spatial pattern of activity in each VLVp. Because the bars are formed by a competitive process, their lengths are always complementary to each other. We call this model the competitive edge model.

The detailed architecture we propose has three classes of neurons in the VLVp with each class having a different distribution along the dorsal-ventral axis. We use this distribution to match the observation of three different cell types in the VLVp [Carr, et al, 1989]. For the ventral cells to inhibit the dorsal end of the opposite VLVp more than they are inhibited, the model has one class of neurons which are more numerous at the ventral end. These are the only neurons in our model which project to the opposite VLVp. Curiously, of the three cell types observed by Carr, two are GAD^+ and so presumably are GABAergic inhibitory neurons, yet the third (GAD^-) type is the type which is more numerous at the ventral end. Thus we would predict that the inhibitory transmitter is not GABA. To dampen the effective positive feedback of this circuit, we have added a class of local inhibitory interneurons. Through simulations we have found that the model works well if this class is more numerous at the dorsal end. The other GAD-positive class serves a function in projecting to other nuclei. We will present the results of simulations after discussing the simulation in detail.

Simulation methods

In this section we present in detail the methods we used to simulate the two VLVps. One of the problems faced in simulating this system is the number of neurons involved, since an entire iso-frequency slab in one VLVp contains roughly 1000 neurons. The total number we actually simulated in an iso-frequency slab is 800. The numbers are clearly rough estimates, but they do demonstrate the need for modelling thousands of neurons.

The model we used for a neuron is a single compartment model obeying the membrane equation

$$C\frac{dv}{dt} = -g_L(v-v_L) - g_E(v-v_E) - g_I(v-v_I) \qquad (1)$$

where v is the cell's membrane potential, v_L, v_E and v_I are fixed reversal potentials for some set of channels, g_L is a fixed passive leakage conductance, and g_E and g_I are excitatory and inhibitory conductances which vary in response to the cell's inputs. The cell's output is in the form of spikes. These spikes are randomly generated with an average rate given by a sigmoidal function of the membrane potential. The effect of arriving action potentials on g_E and g_I is given by modelling them as dynamical variables obeying the equation for a damped harmonic oscillator

$$\frac{d^2g}{dt^2} = -\gamma\frac{dg}{dt} - \omega^2 g \qquad (2)$$

When an excitatory cell fires, it increments dg_E/dt of those neurons to which it projects by an amount which reflects the strength of the connection. Inhibitory neurons behave similarly, except of course they increment dg_I/dt. γ and ω are chosen so that the oscillator is overdamped, so the conductances never become negative. By using this equation, we do not intend to suggest that these conduc-

tances actually have some dynamics, whether modelled well by a harmonic oscillator or not. Rather we simply want to approximately reproduce a post-synaptic potential. When a spike arrives, the conductance first rises, reaches a maximum, and then decays exponentially. The resulting voltage will follow a similar time course (dropping if the spike came from an inhibitory neuron), although it will rise less sharply. The effects of multiple spikes naturally add without having to keep track of when the spikes arrived. The use of spikes greatly increases the speed of the simulation because each neuron does not have to get a value from each of its inputs on every time step. Instead, on each time step a neuron affects other neurons *only* if it is firing on that time step. Otherwise it does not communicate its state to other neurons.

When γ is very large relative to ω, we can use the equation

$$\frac{dg}{dt} = -\gamma g \qquad (3)$$

for additional speed, since it is easier to integrate. In this case, when a cell spikes it increments g_E or g_I rather than dg_E/dt or dg_I/dt. The comments about efficiency of communication and addition of the effects of multiple spikes apply in this case also.

Numerical integration of equation (1) tends to be unstable if Euler's method is used. The ability of more sophisticated general ODE solvers to take larger time steps can't be used, since we need small time steps for several reasons. In principle, spikes can arrive at any time, so the time step length determines the resolution with which this can happen. Also we are interested in following the detailed time development of the system. For these reasons we decided to solve equation (1) analytically with the g's held constant, as in [MacGregor, 1987]. Although equations (2) and (3) are stable when Euler's method is used, we use their analytic solutions also. No doubt faster methods are available, but this is currently adequate.

We could model the output spike train of a neuron as a Poisson process, but this is more random than is realistic. Instead, we generate spikes less randomly by the following procedure. Each neuron has a counter or clock which is incremented on every time step by the product of the length of the time step and the current firing rate of the neuron. When the clock reaches one, a spike is fired and the clock is reset. Randomness is introduced by resetting the clock to a random value within some range of zero. The range of possible values varies linearly with the firing rate, so that at the neuron's maximum firing rate the generated spike train is less random, while at low firing rates the spike train is more random relative to the average inter-spike interval.

A further large increase in speed is achieved by having all neurons of a given type at a given level in a nucleus receive exactly the same input so they will have exactly the same voltage. Thus for each such position we only need to keep track

of one voltage and pair of conductances for all the neurons there. (There is, however, a separate spike generation clock for each neuron.) Since we simulate forty dorsal-ventral positions in each VLVp (the dorsal-ventral length divided by a typical neuron diameter = 1 mm / 25 μm), we only need to integrate differential equations for 80 neurons. The mutual inhibition of the VLVps in the competitive edge model forms a positive feedback loop which is somewhat sensitive to noise. It seemed to us that modelling neurons at one level in the VLVp with the same membrane potential but different spike trains was likely to give a fairly realistic train of spikes inhibiting each VLVp, and so it still allows us to check the probable stability properties of the model.

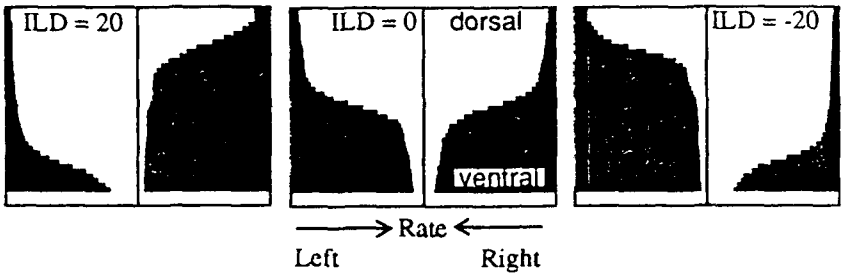

Figure 2. Typical activity pattern of the simulated VLVp. Horizontal lengths of bars indicates percent of maximumfiring rate at that dorsal-ventral position.

Comparison of model with data

Figure 2 shows the spatial patterns of activity in the simulated VLVps. The complementary bars are clear. Figure 3 shows typical ILD response curves of neurons at different dorsal-ventral positions for several ABIs. Comparison with [Manley, et al, 1988] shows good agreement.

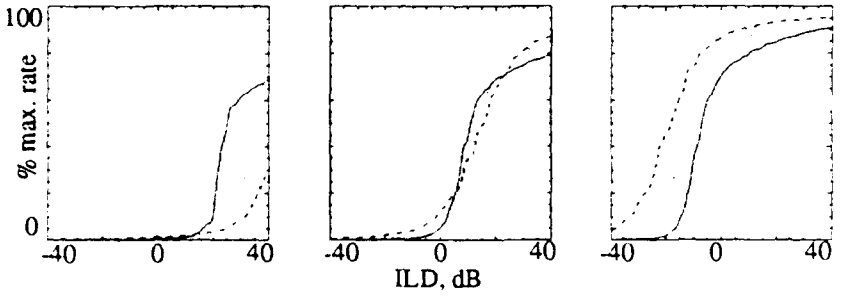

Figure 3. Simulated ILD response curves of VLVp neurons at several ABIs. The left plot is for a dorsal neuron, the center plot is a central neuron, and the right plot is a ventral neuron. Dashed = 40 dB, dotted = 30 dB, solid = 20 dB.

Conclusion

We have presented a model of interaural level difference processing in the barn owl's nucleus VLVp. The responses of neurons to different stimuli in a simulation of this model agree well with the published data. In addition we have presented the details of techniques we used which allow us to simulate 2400 neurons in this system quite rapidly, although we do not claim that our current approach is optimal. These techniques should be relevant for simulating other systems, especially if the details of action potentials are not relevant and information is represented redundantly, i.e. many neurons are expected to have the same response in any given stimulus condition.

Acknowledgments

This work was supported by AFOSR contract F49620-89-C-0131 and DARPA contract F49620-90-C-0010.

References

Carr, C. E., I. Fujita, and M. Konishi. (1989) Distribution of GABAergic neurons and terminals in the auditory system of the barn owl. *The Journal of Comparative Neurology* **286**: 190-207

Knudsen, E.I., G.G. Blasdel, and M. Konishi. (1979) Sound localization by the barn owl measured with the search coil technique. *Journal of Comparative Physiology* **133**:1-11

Konishi, M. (1986) Centrally synthesized maps of sensory space. *Trends in Neurosciences* April, 163-168

MacGregor, R. J. (1987) Neural and Brain Modeling. San Diego, CA: Academic Press

Manley, G. A., C. Köppl, and M. Konishi. (1988) A neural map of interaural intensity differences in the brain stem of the barn owl. *The Journal of Neuroscience* **8**(8): 2665-2676

Moiseff, A. (1989) Binaural disparity cues available to the barn owl for sound localization. *Journal of Comparative Physiology* **164**: 629-636

Spence, C. D. and J. C. Pearson (1990) The computation of sound source elevation in the barn owl, in *Advances in Neural Information Processing Systems* 2, 10-17. San Mateo, CA: Morgan Kaufmann

Takahashi, T. T. (1988) Commissural projections mediate inhibition in a lateral lemniscal nucleus of the barn owl. *Society for Neuroscience Abstracts* **14**: 323

APPENDIX C

Draft Manuscript

DRAFT 11/21/90

Temporal hyperacuity and single neuron selectivity: Microsecond time resolution in a neural compartmental model.

W.E. Sullivan

Department of Ecology and Evolutionary Biology
and
Program in Neuroscience
Princeton University
Princeton, N.J.

Introduction:

An understanding of the precision with which single neurons can perform synaptic operations is of great importance to studies of sensory and motor processes, if we are to ultimately relate behavioral and psychophysical performance to its underlying neuronal mechanisms. There are a number instances of sensory and motor behavior which indicate that nervous systems possess the ability to resolve very small time differences - in the microsecond or sub-microsecond range. These include discrimination of sequential changes in echo delay by bats (10 to 400 nanoseconds: Simmons 1979, Simmons et.al. 1990, Moss and Schnitzler 1989), discrimination of differences in electric organ discharge frequency to that of a jamming stimulus by time domain analysis in electric fish (400 nanoseconds: Carr et.al. 1986, Rose and Heiligenberg 1985), binaural time disparity measurement for horizontal sound localization in owls, bats and humans (10 microseconds: Moiseff and Konishi 1981, Moiseff 1989, Harnischfeger 1980, Harnischfeger et. al. 1985, Blauert 1983), accurate release timing when throwing at a target (100 microseconds: Calvin 1983), or the use of binocular delay for depth perception (160 microseconds: Burr and Ross 1979). All of these thresholds would seem to be too small for single neurons to resolve since neural events take place on millisecond rather than microsecond time scales; and although it is generally assumed that such behavioral 'hyperacuity' involves large neural ensembles, population averaging can only remove noise. That is, in addition to noise, there must also be a signal, and the degree to which single neurons can select for and thereby detect small differences in the timing of their inputs, determines the potential strength of this signal. The present work shows that microsecond time resolution at the cellular level is in fact theoretically possible by demonstrating how this can be achieved in a neural compartmental model. In addition, the results provide an interesting example of serial internal filtering, by which the temporal selectivity in the model's "axon" can be much greater than what would be observed in its "soma".

The Compartmental model:

As shown in figure 1a, the model consists of nine passive electrical compartments designed to simulate the dendrites and soma (Rall 1964) and one or more active compartments containing voltage sensitive conductances modelled using the equations derived by Hodgkin and Huxley (1952) from their voltage clamp experiments on the squid giant

axon. [1] Synaptic input is provided by a time varying conductance linked to an equilibrium battery of 0 mV for excitatory and -70 mV for the inhibitory inputs. The active and passive compartments are linked by a coupling resistor (g_coup). As shown by previous workers (Holden and Yoda 1981; Waxman and Wood 1984, Moore et.al. 1983, Bunow et.al. 1985), the voltage sensitive conductance densities and/or rate constants in the original Hodgkin-Huxley model are insufficient for action potential initiation when connected to a passive load equivalent to that posed by a normally sized cell. In these simulations, a value of 800 mmho/cm2 was used for voltage sensitive sodium conductance. Voltage sensitive potassium conductance was varied from 200 to 1600 mmho/cm2. Similar results are obtained for other choices for maximum sodium conductance, since above a certain level of channel density, the ratio of the two voltage sensitive conductances plays a major role in determining the model's response properties. The voltage sensitive rate constants for opening and closing of the h,m and n gates were factored by 10.0 to simulate an increased temperature (see Moore et.al. 1983). This gives action potential durations of approximately1 millisecond.

Since the purpose of this investigation was to determine the theoretical limits of time resolution rather than to model a specific neuron, no attempt was made to confine internal and membrane properties based on empirical data. There are several important rationales for this choice, the first being that well studied neurons such as motoneurons (Bunow et.al.1985) may or may not be specialized for fine temporal analysis. Secondly, several assumptions are often needed to make compartmental models because a complete measurement of all electrical parameters is difficult to obtain. Nevertheless, reasonable estimates can often be made based on the input resistance and geometry of the modelled neuron (Reference?). However, in an abstract analysis, electrical parameters can be altered by changes in geometry or in the electrical constants of membrane or cytoplasm, both of which may vary over a wide range (Holden and Yoda 1981). Therefore, to reduce the number of variables, the model's electrical parameters were directly modified. It is even arguable that neurons can independently control membrane and internal electrical parameters. For example, while membrane conductance and capacitance are proportional to membrane area, conductance is much more dependent on channel density. Changing the volume of a compartment changes its internal resistance, but this

[1] In should be noted that this traditional view of a passive soma-dendritic tree and an active axon is most likely a severe oversimplification in some cases and simply wrong for many neurons (references on active dendritic). Therefore, it is likely that the results of this abstract analysis could be applied to virtually any location within the neuron.

parameter must also depend on the relative volume of non-conductive elements such as filaments or organelles whose distribution is certainly not uniform. Finally, membrane area can be varied independently of volume by the presence of protrusions or crennelations on the cell surface. Therefore, an analysis of how optimal combinations of electrical parameters could be anatomically implemented may provide insights into the functional properties of well described nerve cell types.

The passive compartment parameters can be obtained assuming a cylinder 5 microns in diameter and 15 microns in length with a specific membrane resistance of 6000 ohm cm^2 and an internal resistivity of 125 ohm cm. This gives a membrane conductance of 0.0008×10^{-6} mho, a membrane capacitance of 0.0016×10^{-9} F and an internal conductance of 1.3×10^{-6} mho. The electrotonic length of each compartment was 0.0194 lambda, well within the range required to assume isopotentiality (Rall 1969).

For each time step, the currents due to transmembrane movements of ions down their electrochemical gradient and to ohmic currents moving between passive compartments were calculated and summed. The net current entering a compartment was then divided by membrane capacitance to obtain the voltage change. For the active compartment, actual currents were calculated for inputs from adjacent compartments and these divided by capacitance to obtain dV due to axial current flow. Since the Hodgkin-Huxley model was derived for a space clamped axon, its electrical constants are expressed in terms of conductance density. The change in voltage for the voltage sensivite and leakage membrane currents were therefore determined separately and added to the voltage change due to axial currents. To avoid oscillations and to maximize the accuracy of the simulations, a small time step (0.1 usec) was used. All programs were written in C and run on a Masscomp MC-5500 computer (Concurrent Computer Corp.).

To investigate temporal selectivity in this model, a coincidence threshold, equivalent to the maximum delay between two subthreshold linearly rising and decaying conductance inputs for which a spike could be produced, was determined for a range of subthreshold inputs (Figure 2). In the initial simulations, a synaptic duration of 1 millisecond was used. Since changes in electrical parameters affect absolute sensitivity, the action potential threshold for a single input pulse was first determined and two subthreshold pulses at levels of 52.5, 55, 60, 75 and 90% of single input threshold were then used to measure the model's temporal selectivity (for pulses equal to or greater than 100% of single input threshold, the system

would be measuring recovery times rather than coincidence selection and if each subthreshold input is 50% of single pulse threshold, they could only produce a spike at 0 time delay by definition). The maximum delay capable of producing a spike represents the sharpness with which coincident events are selected whereas the change in maximum delay with input level measures the tolerance of this temporal sensitivity to variations in synaptic strength. For the present purposes, an 'action potential' is defined as a depolarization in the active compartment with a peak greater than a certain minimum value (-30 mV in this case). As demonstrated in figure 2b, the coincidence threshold is thereby determined from the intersections of curves for time delay vs. peak size with this spike criterion. For models such as this, with a clear all-or-none output (as shown by the nearly vertical rise in output peak height at the coincidence threshold), the choice of spike criterion does not greatly affect the result. In this particular case, coincidence thresholds ranged from 100 to 550 microseconds for input levels of 52.5 to 90% of single pulse threshold.

The effects of variations in several model parameters on temporal selectivity are shown by plotting coincidence threshold for iso-input levels (relative to single pulse threshold) against the parameter of interest (figure 3). This analysis reveals the importance of voltage sensitive potassium channel density, leakage conductance in the active compartment and the coupling conductance separating the active and passive compartments. Increasing the density of voltage sensitive potassium channels causes a decrease in coincidence threshold at all relative input levels as well as a compression of the tuning function by a greater reduction of higher input levels. Increasing the leakage conductance in the active compartment can also have a profound influence on temporal tuning. However, because the changes due to variations in any one parameter can be affected by the values of other parameters, it is difficult to quantitate these effects. This is especially true of active-to-passive coupling conductance, which was found to be positively correlated with temporal tuning when leakage conductance in the active compartment is large but not correlated or negatively correlated for medium or low leakage conductances. Inhibition in the passive compartments can cause sharpened temporal tuning in some models but has little effect on others. Nevertheless, these analyses do suggest some parameter combinations for which sharp tuning can be obtained and provide an explanation for the mechanism by which it is achieved.

For single active compartments, sharp temporal selectivity was achieved by combining a relatively small active-to-passive coupling conductanc-

with high voltage sensitive potassium and leakage conductances in the active compartment. For an action potential to be generated under these conditions, the active compartment must be rapidly depolarized to enable sufficient sodium channel activation for sustained regenerative feedback before hyperpolarizing currents due to increased leakage driving force and potassium channel activation are able to repolarize the membrane and shut this process off. By controlling the flow of current into the active compartment, smaller coupling conductances make rapid depolarization in the passive compartments even more critical. As might be expected, all of these parameters cause the synaptic conductance threshold to be raised (see figure 4c), so that in the most temporally sensitive models, the synaptic conductance essentially clamps the passive membrane potential to the synaptic equilibrium and the difference between subthreshold and suprathreshold inputs has more to do with the rate at which this saturating potential is reached rather than with the final voltage level voltage that is achieved. In the original Hodgkin-Huxley model, action potential generation is goverened by a dynamic threshold in that the voltage level at which a spike is discharged depends on the rate at which the cell is depolarized.[2] These simulations therefore suggest that fine temporal acuity can be achieved by changing from a threshold that is largely determined by voltage level to one which is dominated by depolarization rate.

Graded responses of single compartment models with small coincidence thresholds:

In models with a single active compartment, reductions in coincidence threshold were accompanied by shifts from an all-or-none output to a more graded response. As shown in figure 4, for models with small active-to-passive coupling conductances, increases in leakage conductance in the active compartment produce significant changes in coincidence threshold, but this is accompanied by a flattening of the output peak vs. delay function (bottom). Models with larger coupling conductances display a more severe flattening such that at very large leakage conductances, the difference between subthreshold and suprathreshold responses is

[2] Although Hodgkin and Huxley postulated such rate accomodation, subsequent work by Jakobsson and Guttman (1980) and by Rinzel and Baer (1988) showed that given the original gNa max and gK max parameters of 120 mmho/cm2 and 36 mmho/cm2, rate accomodation is not seen no matter how slowly the membrane is depolarized and in fact a "reverse" accomodation is seen for very slow membrane depolarizations. Thus, it clear that potassium channel density can cause both quantitative and qualitative changes in rate accomodation.

essentially arbitrary. This reduction in all-or-none behavior accompanied improvements in temporal discrimination irrespective of the parameter changes used to achieve them.

Models with more than one active compartment:

Since a model with a single active compartment is quite unrealistic, the effects of adding more active compartments to the model were investigated. As shown in figure 5, this can produce dramatic improvements in both tuning sharpness and subthreshold- suprathreshold discrimination. The results from multiple compartment simulations suggest that the graded nature of the response in the initial active compartment can in turn be filtered according to rise rate and/or peak by successive active compartments. By placing such "temporal filters" in series, significant improvements in temporal accuracy can be achieved. In addition, because the distal compartments are more electrically isolated from the soma, improvements in spike height and in the contrast between sub- and suprathreshold responses can also occur. This is illustrated by the 4 active compartment model in which the distal compartment (labeled "axon") differs from the three proximal active compartments by having fewer voltage sensitive potassium and leakage channels (see legend for details). This model fires large (+30 mV peak) spikes with coincidence thresholds from 1.5 to 48 microseconds for 52.5% to 90% input pairs. The output of this model is shown for time delays of 1.0 and 2.0 microseconds for two inputs at the 52.5% level, the first of which produces a spike in the distal compartment, whereas the second does not. However, in both cases, spikes are seen in the first two compartments. This is because the threshold for producing a spike in the distal compartment is greater than that for producing an aborted spike in the proximal compartments. Therefore, there is no delay tuning in the proximal compartments while an extremely sharply tuned response is seen distally. Although on the scale of the figure, spikes in the proximal compartments appear to be identical in the subthreshold and suprathreshold cases, there is actually a very slight difference in the rate of rise and peak height between the two conditions. Interestingly, the third active compartment shows a graded response to all input conditions. The final active compartment has fewer potassium channels than the 3 proximal compartments and is thereby capable of firing a large spike if the graded potential in its proximal neighbor is sufficiently large. Temporal filtering in the proximal compartments has therefore converted a very small change in input timing to a graded potential in the 3rd active compartment, to which the last compartment can respond, using a more or less conventional voltage threshold.

Effects of synaptic input width on temporal tuning:

Although the foregoing results suggest that fine temporal discrimination is possible without postulating very brief synaptic inputs (since all of the results described previously were obtained with input durations of1 millisecond), it was nevertheless of interest to determine how changes in synaptic duration would affect temporal selectivity. When this was tested on a model with one active compartment, decreases in synaptic duration were accompanied by decreases in coincidence tuning, but the decrease in temporal tuning was less than the decrease in synaptic width (figure 6a). Furthermore, below about 200 microseconds duration, coincidence tuning increased rather than decreased. This would suggest that very accurate time resolution is not achieved simply by reducing the time window of post-synaptic conductance change. This point is further amplified by examining tuning changes with synaptic duration in the 4 compartment model described above. In this case, changes in synaptic duration from 2000 to 250 microseconds had virtually no effect of coincidence tuning thresholds, and at 100 microseconds duration, the threshold dramatically increased (figure 6b). What did change in these simulations was single input threshold which *decreased* as input width was shortened (figure 6c). This result clearly implicates the rate of rise (since shorter triangular pulses have a steeper rise and fall) rather than duration as a critical factor in temporal discrimination. That is, from a pre-synaptic perspective, synchrony of release rather than release duration or mechanisms for synaptic transmitter removal (such as transmitter degredation or rapid reuptake) is critical for temporal discrimination.

Discussion:

Although the results presented herein provides an explanation for temporal hyperacuity in terms of single unit responses, some caution is clearly required. In the first place, there is a growing body of evidence to suggest that the resolution which can be demonstrated at single neuron levels may not actually be used. For example, rods have been shown to have a measurable response to a single photon (Barlow et.al. 1971, Baylor et.al. 1979), but this level of illumination is well below behavioral threshold since in a natural situation, there is no way to "average" the input over space or time if only a single photon is present. From a bit higher up in the visual pathway is the demonstration by Shapley and Victor (1986) that retinal ganglion cells can respond to displacements of a sinusoidal grating over a small fraction of their receptive field with a resolution which may exceed psychophysical measurements of vernier

hyperacuity. In a third example from the visual system, Newsome et.al. (1989) have shown that some neurons in the extrastriate visual area MT are able to detect global movement in a random dot display at a lower signal-to-noise ratio than could the monkey they were recorded from. All of these examples make clear that the problem of behavioral hyperacuity is not so much a problem of neuronal resolution as it is a problem of neuronal noise. The present analysis extends this argument to the time domain by showing that fine temporal resolution is theoretically possible even if synaptic conductance changes and action potentials have relatively leisurely time courses. Clearly then, a temporal signal at the level of behavioral thresholds can exist in neural responses. However, it is also important to consider how the most efficient system could be achieved given the problems of noise and of obtaining a complete representation of the behaviorally relevent range. These considerations would suggest that even if very fine temporal resolution is possible, it may be impractical and that the best solution may involve improvements in signal-to-noise both by averaging and by improved resolution at the single neuron level.

One way of analyzing the problem is to consider the amount of information that a detector conveys over time - that is the information rate of the cell's output (Shannon and Weaver 1949, Barlow 1972). A detector may signal the probability that an event to which it is tuned has occurred by firing, or that this event has <u>not</u> occurred by remaining silent. The more sharply tuned the detector is, the more information it gives when it fires, but it gives less information by being silent because there is a wider range of conditions to which it is insensitive. A sharply tuned detector therefore would give very precise information when it fires but since the event may occur rarely, the net information rate of the detector may be low. Conversely, if tuning is very broad, then information rate is low due to the wide range of stimulus values that could evoke the same discharge rate given a moderate amount of noise. If evolution optimizes the amount of information per unit time that nerve cells can transmit, then it seems likely that some intermediate level of tuning sharpness would be selected.

Another way to conceptualize the problem of representation and efficiency is to consider the number of neurons that are needed for a solution. If tuning properties of single neurons are poor and very fine resolution is needed, then the nervous system must contain a considerable amount of redundancy to improve the signal-to-noise ratio. Information theory shows that the S/N improves as the square root of the number of channels used to carry the signal (Reference?). An alternate strategy suggested by the present results would be to improve the acuity of single

cells. This strategy runs into difficulties because as tuning width decreases, more cells are needed to cover the same behaviorally relevant range. However, in this case, the number of neurons required does not increase as the square of the desired improvement in S/N, rather it is proportional to S/N directly. That is, we need 100 neurons to improve resolution by a factor of 10 using averaging but only10 neurons to improve resolution if these cells have tuning widths which are 1/10 as wide. This argument presupposes however that some form of interpolation is used to create the final percept and if this is the case, then sharpening of single unit tuning functions is clearly desirable because it is more efficient than averaging. An alternative scheme whereby the output of tuned receptors is summed according to rank within the array to create a monotonic parameter code suggests to the contrary that broad tuning is desired (Baldi and Heiligenberg 1988).

Another problem with very sharp coincidence detectors is that input noise or jitter can render their outputs less effective in terms of information quality since stray coincident inputs can occur by chance or what should be coincidences can be missed. This is especially true if temporal tuning is as sharp or sharper than the average scatter in input timing. One way to avoid this problem is to assume that the input functions used in the present simulations represent the sum of a population rather than of single synapses. Nevertheless, if input scatter is large, then a large convergence is needed and the advantages of sharp tuning over averaging may be lost, since both are in fact required. In this situation, it may be more efficient to match the tuning of the coincidence detector to the amount of jitter in the input doing some averaging at the input and some on the output. In addition to averaging done in parallel (i.e. by redundancy), it is also useful to consider a serial scheme whereby jitter is removed in stages so that sharper detectors can be built more centrally given that jitter has been removed in prior processing stages (Carr et.al. 1986). In other words, a serial filtering scheme for sharpening temporal codes could operate both within single cells (see below) and along a processing stream.

The above discussion suggests that both population averaging and improved single unit temporal selectivity are likely to be employed in systems which have achieved fine temporal resolution. While efficiency might be a metric by which to predict how much of each should be found, there is also serendipity to consider - the 'best' system from an engineering standpoint is not always the solution that evolution has found (Heiligenberg 1987). Nevertheless, the algorithm used by bats to

discriminate jittering echo delays with a precision of 10 nanoseconds, must be fairly close to perfection (Simmons et.al. 1990).

Possible cellular mechanism for temporal sharpening and some implications for electrophysiologists:

The simulation results of the present study suggest that sharp temporal tuning can be achieved if rate accomodation is maximized so that only very rapid inputs are capable of generating a response. In addition, this process of selection for rapidly rising inputs can be carried out in series so that distal segments of an active process such as an axon can show much finer temporal selectivity than do more proximal segments. Clearly, the true or functional outputs of a neuron are those which affect transmitter release at its synaptic endings, not those which can be observed at the soma. In this respect, inhomogeneities in the axon have long been suspected as potential sources of information "post-processing" (Parnas 1972, Waxman 1972, Goldstein and Rall 1974, Parnas et.al. 1976, Moore and Westerfield 1983, Bunow et.al. 1985) in contrast to the pre-processing assumed to be performed by the dendritic tree. If such mechanisms are widely employed in the nervous system, then we must reevaluate our neurophysiological data since recordings taken from the soma (whether intracellular or extracellular) may suggest that temporal tuning is very broad or even nonexistent, when in fact it is quite sharp. Unfortunately, theory alone can only point out what may be true, leaving the burden of proof or disproof to the experimenter. At the same time, we must be aware of the biases inherrent in present electrophysiological methods (such as the relative ease of recording from soma as opposed to synaptic endings or axonal nodes) so as to avoid any false sense of security in the conclusions which we draw from them. These considerations also lend further credence to the notion that 'behavioral hyperacuity' may be a misnomer to the extent that it de-emphasizes the potential processing power and precision which might exist at the cellular level.

References:

Baldi, P. and W. Heiligenberg (1988) How sensory maps could enhance resolution through ordered arrangements of broadly tuned receivers. Biol. Cybern. 59: 313-318.

Barlow, H.B. (1972) Single units and sensation: A neuron doctrine for perceptual psychology? Perception 1: 371-394.

Barlow, H.B., W.R. Levick and M. Yoon (1971) Responses to single quanta of light in retinal ganglion cells of the cat. Vision Res. 3: 87-101.

Baylor, D.A., T.D. Lamb and K.-W. Yau (1979) Responses of retinal rods to single photons. J. Physiol. 288: 589-611.

Blauert, J. (1983) Spatial Hearing. MIT Press, Cambridge.

Bunow, B., I. Segev and J.W. Fleshman (1985) Modelling the electrical behavior of anatomically complex neurons using a network analysis program: Excitable membrane. Biol. Cybern. 53: 41-56.

Burr, D.C. and J. Ross (1979) How does binocular delay give information about depth? Vision Res. 19: 523-532.

Calvin, W.H. (1983) A stone's throw and its launch window: Timing precision and its implications for language and Hominid brains. J. Theor. Biol. 104: 121-135.

Carr, C.E., W. Heiligenberg and G.J. Rose (1986) A Time-comparison circuit in the electric fish midbrain. I. Behavior and physiology. J. Neurosci. 6: 107-119.

Goldstein, S.S. and W. Rall (1974) Changes of action potential shape and velocity for changing core conductor geometry. Biophys. J. 14: 731-757.

Harnischfeger, G. (1980) Brainstem units of echolocating bats code binaural time differences in the microsecond range. Naturwissenschaften 67: 314-316.

Harnischfeger, G., G. Neuweiler and P. Schlegel (1985) Interaural time and intensity coding in superior olivary complex and inferior colliculus of the echolocating bat *Molossus ater*. J. Neurophysiol. 53: 89-109.

Heiligenberg, W. (1987) Central processing of sensory information in electric fish. J. Comp. Physiol. 161: 621-631.

Hodgkin, A.L. and A.F. Huxley (1952) A quantitative description of membrane current and its application to conduction and excitation in nerve. J. Physiol. 117: 500-544.

Holden, A.V. and M. Yoda (1981) The effects of ionic channel density on neuronal function. J. Theoret. Neurobiol. 1: 60-81.

Jakobsson, E. and R. Guttman (1980) The standard Hodgkin-Huxley model and squid axons in reduced external Ca^{++} fail to accomodate to slowly rising currents. Biophys. J. 31: 293-298.

Moiseff, A. and M. Konishi (1981) Neuronal and behavioral sensitivity of binaural time differences in the owl. J. Neurosci. 1: 40-48.

Moiseff, A. (1989) Bi-coordinate sound localization by the barn owl. J. Comp. Physiol. 164: 637-644.

Moore, J.W. and M. Westerfield (1983) Action potential propagation and threshold parameters in inhomogeneous regions of squid axons. J. Physiol. 336: 285-300.

Moore, J.W., N. Stockbridge and M. Westerfield (1983) On the site of impulse initiation in a neurone. J. Physiol. (Lond.) 336: 301-311.

Moss, C.F. and H.-U. Schnitzler (1989) Accuracy of target ranging in echolocating bats: Acoustic information processing J. Comp. Physiol. 165: 383-393.

Newsome, W.T., K.H. Britten and J.A. Movshon (1989) Neuronal correlates of a perceptual decision. Nature 341: 52-54.

Parnas, I. (1972) Differential block at high frequency of branches of a single axon innervating two muscles. J. Neurophysiol. 35:903-914.

Parnas, I., S. Hochstein and H. Parnas (1976) Theoretical analysis of parameters leading to frequency modulation along an inhomogeneous axon. J. Neurophysiol. 39: 909-923.

Rall, W. (1964) Theoretical significance of dendritic trees for neuronal input-output relations. In: "Neural Theory and Modelling", R.F. Reiss, ed. Stanford University Press, Stanford Ca., pp. 73-97.

Rall, W. (1969) Time constants and electrotonic length of membrane cylinders and neurons. Biophys. J. 9: 1483-1508.

Rinzel, J. and S.M. Baer (1988) Threshold for repetitive activity for a slow stimulus ramp: A memory effect and its dependence on fluctuations. Biophys. J. 54: 551-555.

Rose, G. and W. Heiligenberg (1985) Temporal hyperacuity in the electric sense of fish. Nature 318: 178-180.

Shannon, C.E. and W. Weaver (1949) *The Mathematical Theory of Communication*. University of Illinois Press, Urbana.

Shapley, R. and J. Victor (1986) Hyperacuity in cat retinal ganglion cells. Science 231: 999-1002.

Simmons, J.A. (1979) Perception of echo phase information in bat sonar. Science 204: 1336-1338.

Simmons, J.A., M. Ferragamo, C.F. Moss, S.B. Stevenson and R.A. Altes (1990) Discrimination of jittered sonar echoes by the echolocating bat, Eptesicus fuscus: The shape of target images in echolocation. J. Comp. Physiol. (in press).

Waxman, S.G. (1972) Regional differentiation of the axon: A review with special reference to the concept of the multiplex neuron. Brain Res. 47: 269-288.

Waxman, S.G. and S.L. Wood (1984) Impulse conduction in inhomogeneous axons: Effects of variation in voltage-sensitive ionic conductances on invasion of demyelinated axon segments and preterminal fibers. Brain Res. 294: 111-122.

Figure Legends:

Figure 1: Shows a schematic diagram for the compartmental model used in these simulations. The model has nine passive compartments and one or more active compartments. The passive compartments are modelled on a cylinder 5 microns in diameter and 15 microns in length. Using R_m = 6000 Ohm-cm, R_i = 125 ohm-cm^2 and C_m = 1.0 μF/cm^2 gives $g_r = 0.0008 \times 10^{-6}$ mho, $c_m = 0.0016 \times 10^{-9}$ F and $g_i = 1.3 \times 10^{-6}$ mho. The synaptic equilibrium battery for excitation was 0 mV and the inhibitory battery was -70 mV. Resting membrane potential was -60 mV. In the active compartment, the Na^+ battery was +55 mV and the K^+ battery -70 mV. Following Hodgkin and Huxley, the resting membrane equilibrium was -50 mV. All other parameters were varible and are listed where appropriate.

Figure 2: Paradigm for studying the temporal selectivity of the model. (A) A linearly rising and falling excitatory synaptic conductance change was applied to passive compartment P2. First, the minimum peak conductance for a particular duration (1 msec in this case) for which a spike could be produced was determined. A spike is defined as a voltage excursion in the most distal active compartment which exceeds a spike criterion level. After measuring single input threshold, two subthreshold pulses whose sum is greater than threshold were used to measure the maximum time separation that will cause a spike. (B) Plots the peak voltage in the distal active compartment as a function of time delay for the standard subthreshold pair levels of 52.5, 55, 60, 75 and 90 % of single pulse threshold. (C) The intersection of the response curves with spike criterion level generates a curve of % single input threshold vs time or a coincidence threshold curve.

Figure 3: Temporal tuning measured with different model parameters. In each figure, coincidence threshold for each level (i.e. 52.5%, 55% etc) is plotted against the model parameter of interest. (A) Coincidence thresholds vs. maximum potassium conductance in the active compartment ($g_{na\ max}$ = 800 mmho/cm^2, g_{leak} = 0.3 mmho/cm^2, $g_{coup} = 0.008 \times 10^{-6}$ mho). (B) Change in inhibitory synaptic conductance in compartment P2. ($g_{na\ max}$ = 600 mmho/cm^2, $g_{k\ max}$ = 200 mmho/cm^2, g_{leak} = 0.3 mmho/cm^2, $g_{coup} = 0.064 \times 10^{-6}$ mho). (C) Change in leakage conductance in active compartment ($g_{na\ max}$ = 800 mmho/cm^2, $g_{k\ max}$ = 600 mmho/cm^2, $g_{coup} = 0.008 \times 10^{-6}$ mho). (D-F) Change in coupling conductance between active and passive compartments. ($g_{na\ max}$ = 800 mmho/cm2, $g_{k\ max}$ = 600

mmho/cm^2, D: g_{leak} = 0.3 mmho/cm^2, E: g_{leak} = 3.0 mmho/cm^2, F: g_{leak} = 30.0 mmho/cm^2).

Figure 4: Change in temporal tuning of single compartment model with increases in leakage conductance in active compartment. (A) Response peak vs. Time delay for different levels of leakage conductance as shown in insert. (B) The same data shown in (A) is replotted relative to coincidence or delay threshold. (Parameters: $g_{na\ max}$ = 800 mmho/cm^2, $g_{k\ max}$ = 600 mmho/cm^2, g_{coup} = 0.008 x 10^{-6} mho).

Figure 5: Model with more than one active compartment showing the changes in temporal tuning as more compartments are added. (A) shows a schematic diagram of the changes in the model. The model diagrammed at the bottom differs from the top three in the design of its distal compartment A4. (A1 - A3: $g_{na\ max}$ = 800 mmho/cm^2, $g_{k\ max}$ = 600 mmho/cm^2, g_{leak} = 20 mmho/cm^2. A4: $g_{na\ max}$ = 800 mmho/cm^2, $g_{k\ max}$ = 400 mmho/cm^2, g_{leak} = 3.0 mmho/cm^2 . g_{coup} between all active compartments = 0.008 x 10^{-6} mho). (B) Shows peak response vs. time delay for the 52.5% level of input for the models shown in A. The extremely sharp tuning displayed by the model with 3 active compartments + "axon" is documented in (C) and (D) where the response at delays of 1.0 and 2.0 μsec respectively is shown. The curves from left to right in each figure are the voltages calculated in compartments A1 to A4 respectively.

Figure 6: (A) and (C) show coincidence threshold iso-level functions vs. synaptic duration for a single compartment model (A) and the 4 compartment model shown in figure 5 (C). (B) and (D) demonstrate the shape of the threshold pulses at different durations for these two models. In the 4 compartment model, the threshold conductance peak is proportional to synaptic duration suggesting that depolarization rate is critical for a response. At the same time, the threshold has increased by a factor of 100.

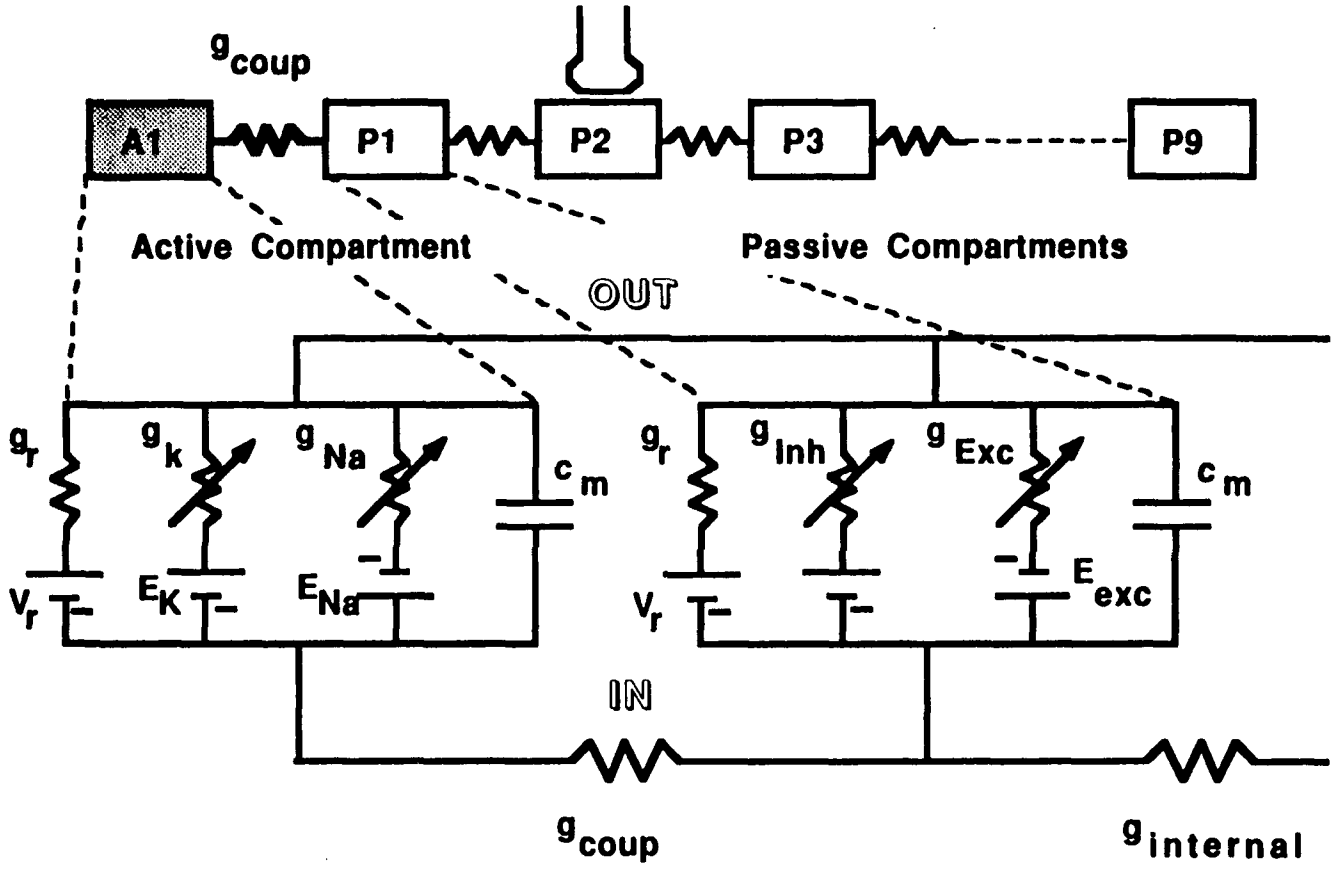
g_{coup}
A1
P1
P2
P3
P9
Active Compartment
Passive Compartments
OUT
g_r
g_k
g_{Na}
c_m
V_r
E_K
E_{Na}
g_r
g_{Inh}
g_{Exc}
c_m
V_r
E_{exc}
IN
g_{coup}
$g_{internal}$

Fig. 1

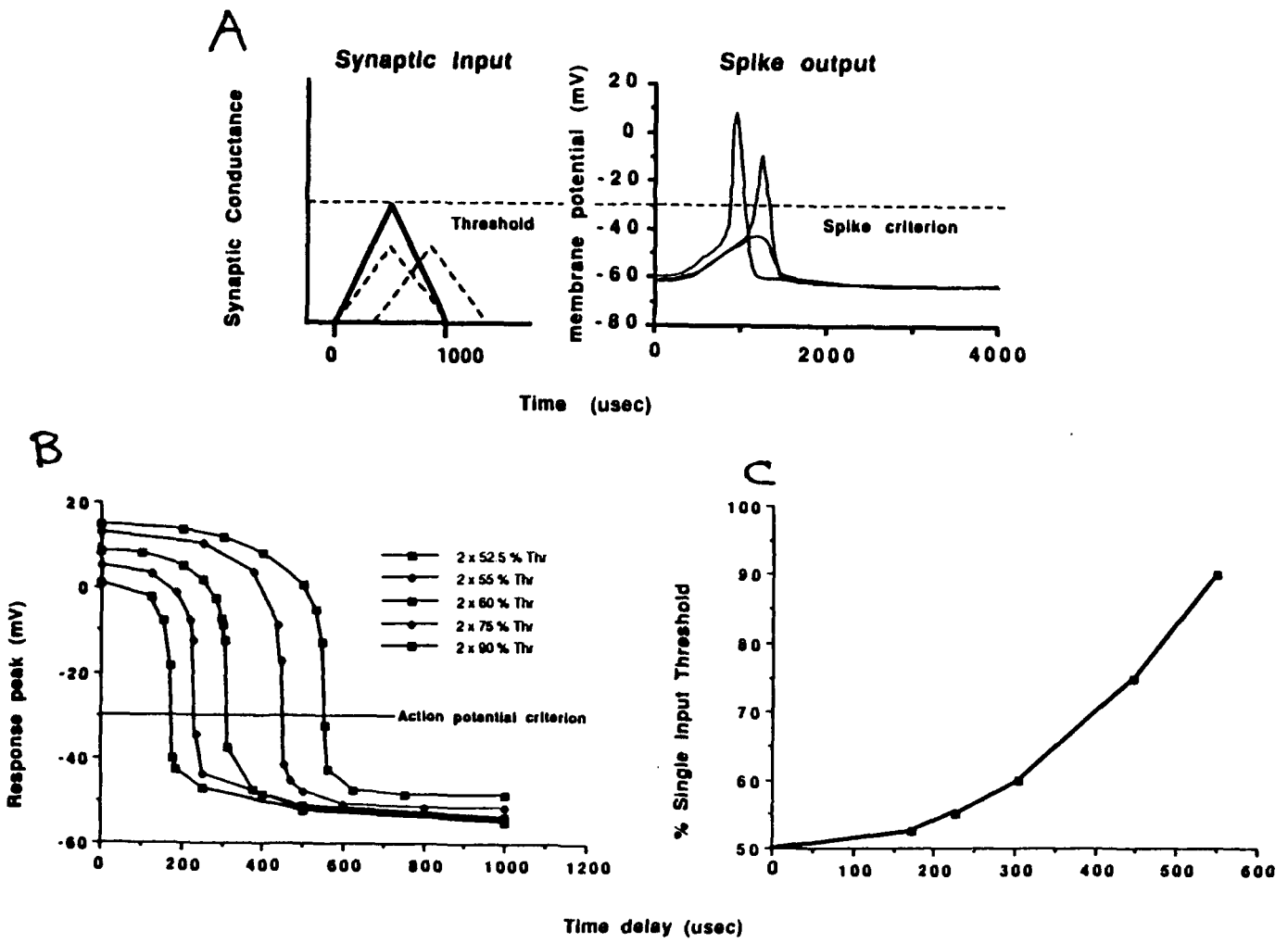
A
Synaptic Input
Spike output
Synaptic Conductance
membrane potential (mV)
Threshold
Spike criterion
20
0
-20
-40
-60
-80
0
1000
2000
4000
Time (usec)
B
C
Response peak (mV)
2 x 52.5 % Thr
2 x 55 % Thr
2 x 60 % Thr
2 x 75 % Thr
2 x 90 % Thr
Action potential criterion
20
0
-20
-40
-60
0
200
400
600
800
1000
1200
% Single Input Threshold
100
90
80
70
60
50
0
100
200
300
400
500
600
Time delay (usec)

Fig. 2

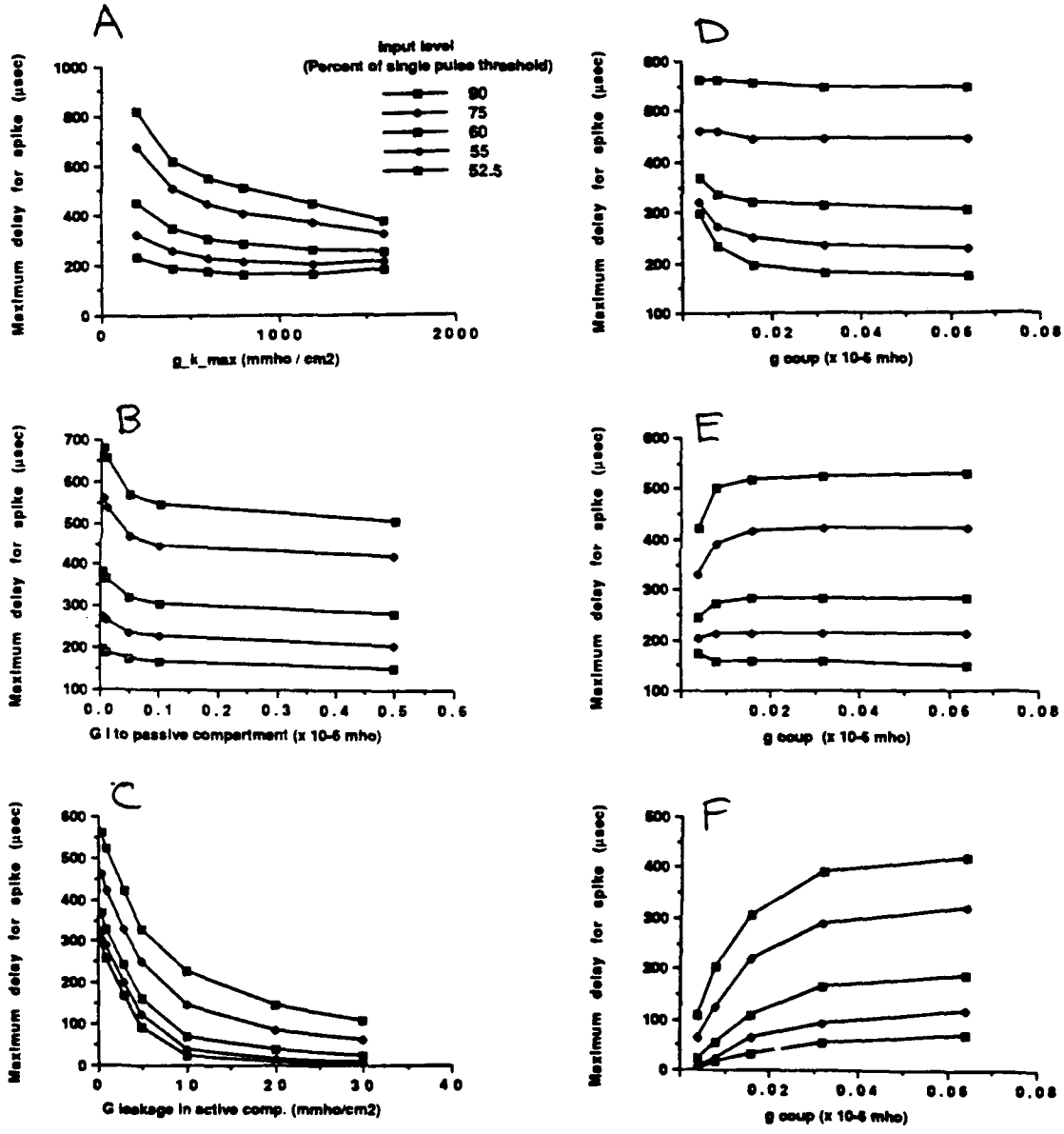
A
Input level
(Percent of single pulse threshold)
90
75
60
55
52.5
Maximum delay for spike (µsec)
g_k_max (mmho / cm2)
B
G l to passive compartment (x 10-6 mho)
C
G leakage in active comp. (mmho/cm2)
D
g coup (x 10-6 mho)
E
g coup (x 10-6 mho)
F
g coup (x 10-6 mho)

Fig. 3

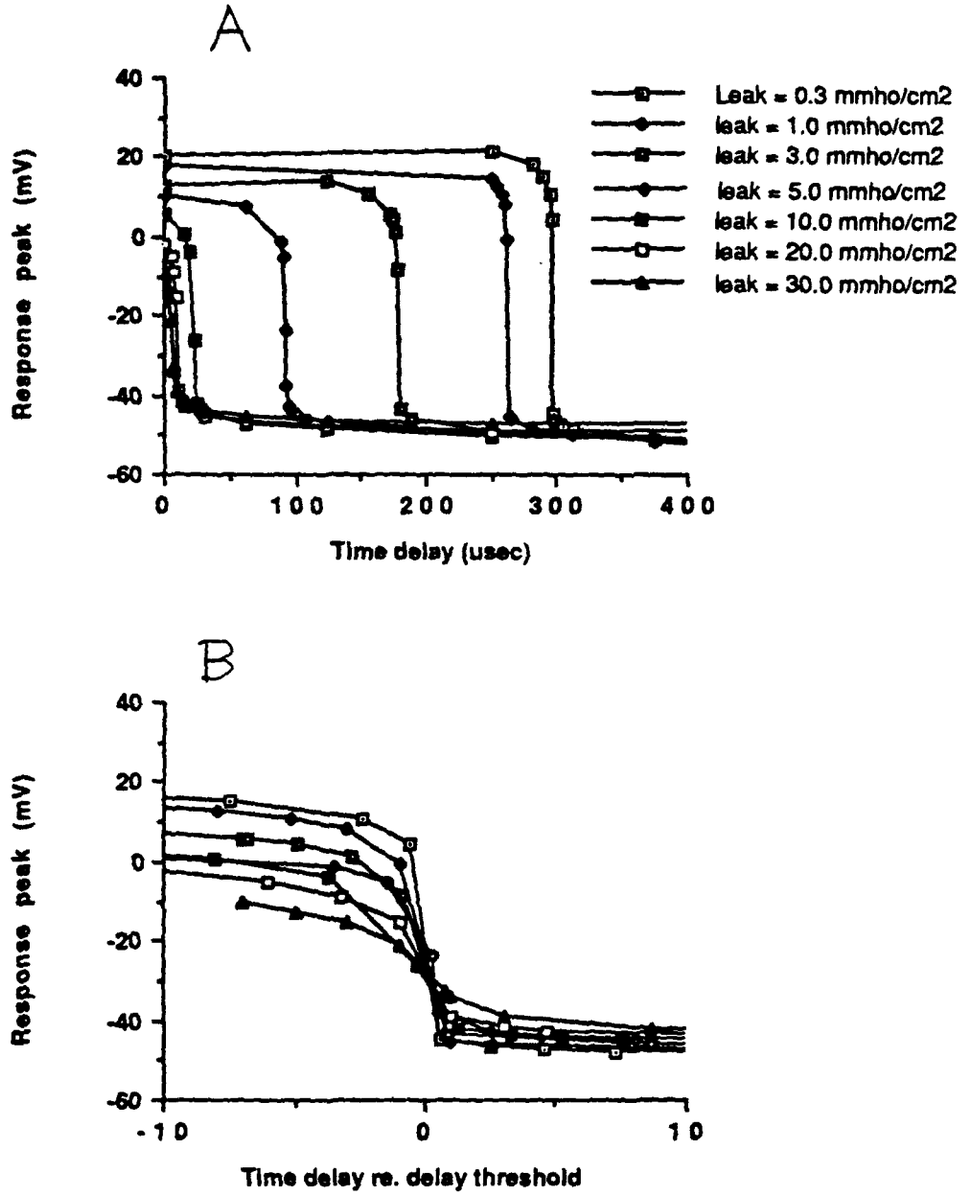
A
Response peak (mV)
40
20
0
-20
-40
-60
0
100
200
300
400
Time delay (usec)
Leak = 0.3 mmho/cm2
leak = 1.0 mmho/cm2
leak = 3.0 mmho/cm2
leak = 5.0 mmho/cm2
leak = 10.0 mmho/cm2
leak = 20.0 mmho/cm2
leak = 30.0 mmho/cm2
B
Response peak (mV)
40
20
0
-20
-40
-60
-10
0
10
Time delay re. delay threshold

Fig. 4

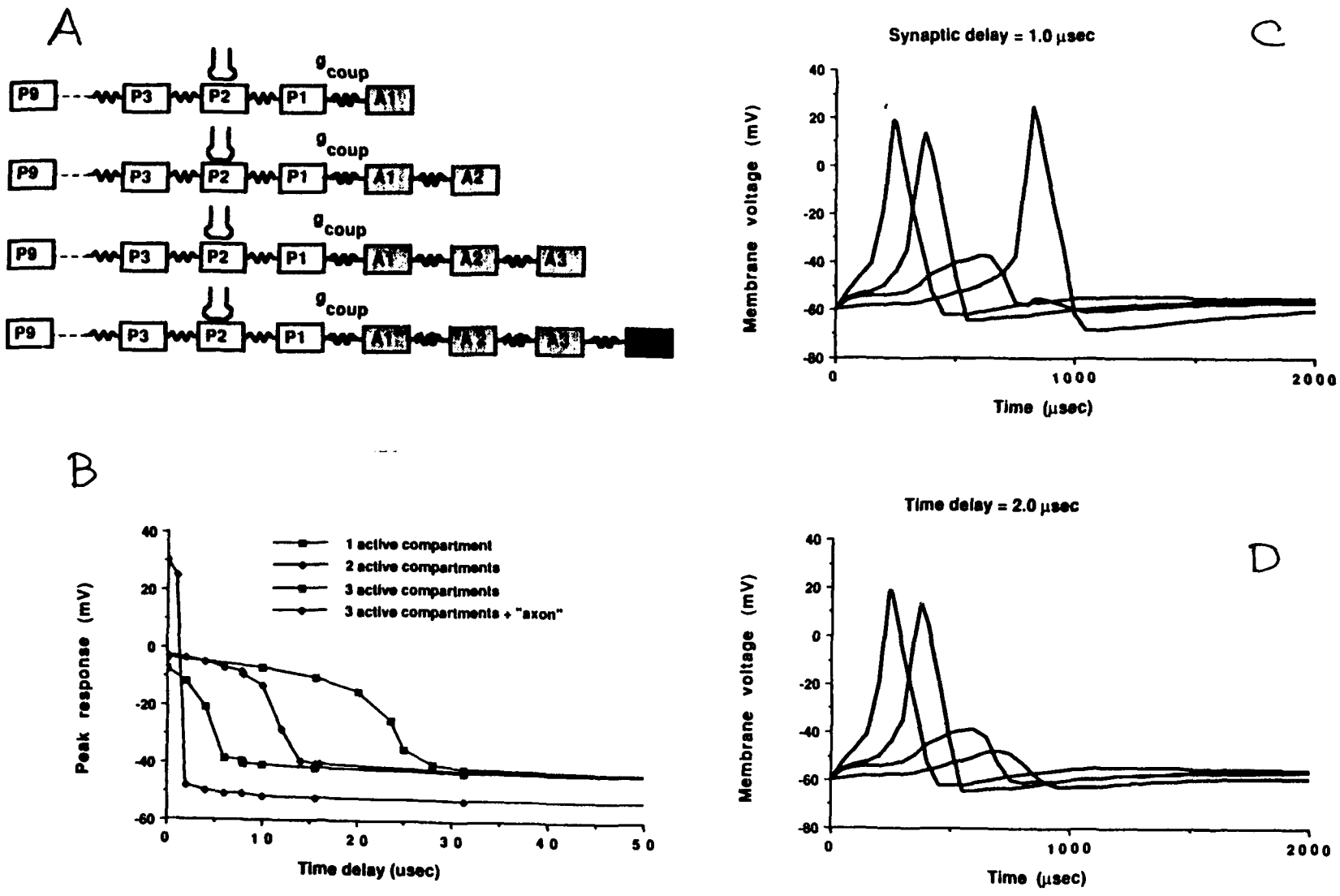
A
P9
P3
P2
P1
A1
A2
A3
g_{coup}
B
Peak response (mV)
Time delay (usec)
1 active compartment
2 active compartments
3 active compartments
3 active compartments + "axon"
C
Synaptic delay = 1.0 μsec
Membrane voltage (mV)
Time (μsec)
D
Time delay = 2.0 μsec
Membrane voltage (mV)
Time (μsec)

Fig. 5

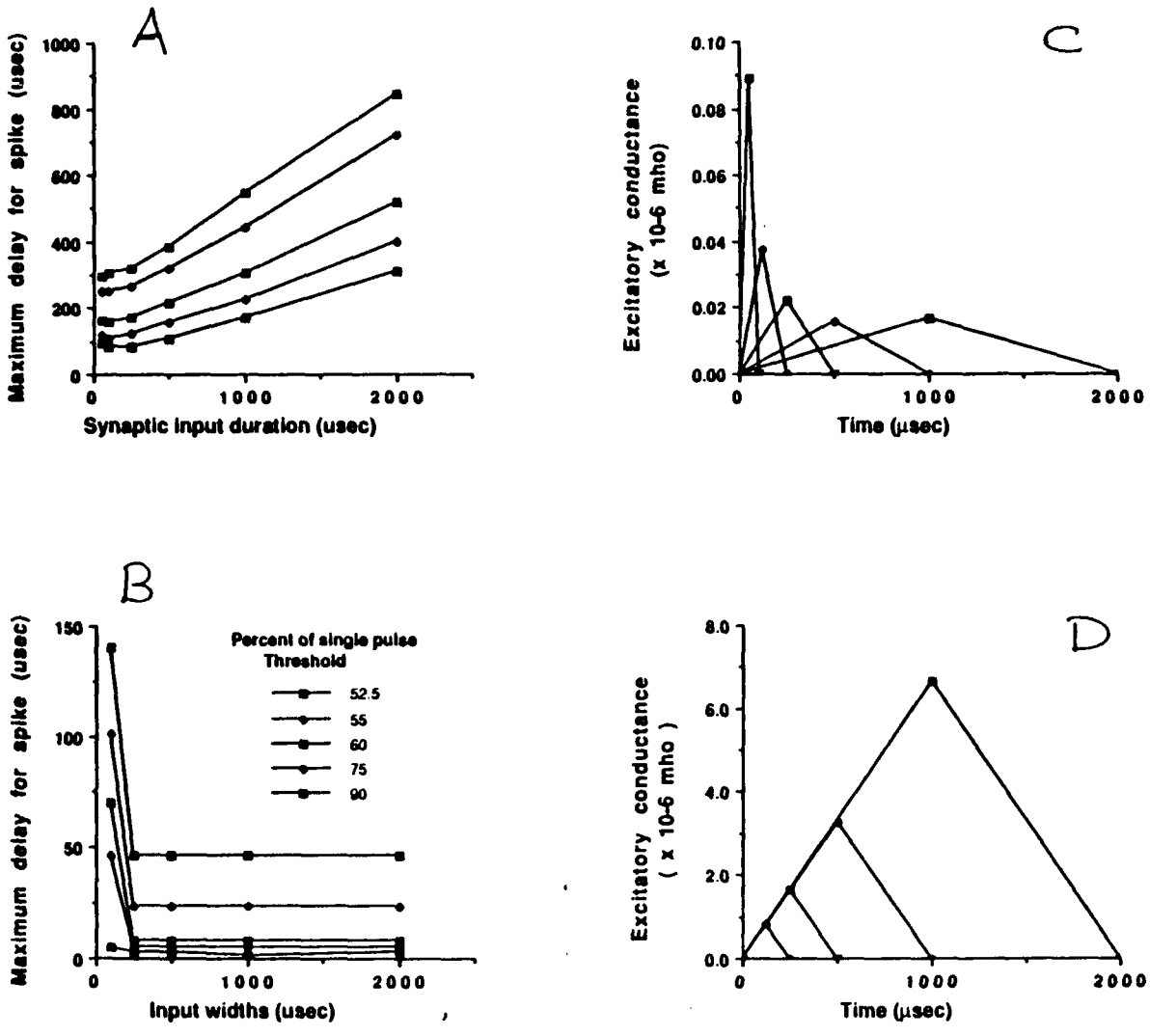
A
Maximum delay for spike (usec)
1000
800
600
400
200
0
0
1000
2000
Synaptic input duration (usec)
C
Excitatory conductance
(x 10-6 mho)
0.10
0.08
0.06
0.04
0.02
0.00
0
1000
2000
Time (µsec)
B
Maximum delay for spike (usec)
150
100
50
0
Percent of single pulse
Threshold
52.5
55
60
75
90
0
1000
2000
Input widths (usec)
D
Excitatory conductance
(x 10-6 mho)
8.0
6.0
4.0
2.0
0.0
0
1000
2000
Time (µsec)

Fig. 6